

The Possible Therapeutic Effect of Mesenchymal Stem Cells and their Exosomes on Experimentally Induced Diabetic Retinopathy in Rats: Histological and Immunohistochemical Study

Original
Article

Heba Elsayed Abd El-Halim, Omayma Kamel Helal, Nessrein Ebrahim Salem, Nahla El-Erakly El-Azab

Histology and Cell Biology Department, Faculty of Medicine, Banha University

ABSTRACT

Background: Diabetic retinopathy (DR) is one of the most common microvascular complication of diabetes that affects the retina and causes acquired blindness among working-age people. Stem cell therapy and exosomes have become promising therapeutic strategies for DR with the development of modern medical technology in the field of cell therapy.

Objective: To evaluate the possible potential therapeutic effect of bone marrow derived Mesenchymal stem cells (BMMSCs) and their exosomes (BMMSCs-exosomes) on induced diabetic retinopathy in rats.

Materials and Methods: Ten young rats were used to prepare mesenchymal stem cells (MSCs). Sixty-four adult male albino rats were divided into six groups. Group I (Control group). Group II (affected group): Rats received single intraperitoneal injection of STZ (60 mg/kg body weight), freshly dissolved in citrate buffer. Group III: DR treated with BMMSCs. Group IV: DR treated with BMMSCs-exosomes. Group V: DR treated with BMMSCs and MSCs-exosomes. Group VI (recovery group). Retinal specimens were taken and processed for histological and immunohistochemical examination.

Results: Group II and VI displayed decreased retinal thickness, obvious disorganization of the outer segment of photoreceptors, together with cytoplasmic vacuolations in the cells of the inner nuclear and ganglionic layers. Furthermore, there was a significant increase ($P < 0.05$) in VEGF and vimentin immunorexpression. Groups III and IV showed improvement of some histological microscopic changes described in group II. While, group V displayed histological architecture and ultrastructure near to control group.

Conclusion: MSCs and exosomes can treat diabetic retinopathy. However, better results can be obtained when exosomes were given with MSCs.

Received: 13 October 2019, **Accepted:** 03 November 2019

Key Words: Diabetic retinopathy, MSCs, exosomes, VEGF and vimentin.

Corresponding Author: Heba Elsayed Abd El-Halim, MB.BCH, Histology and Cell Biology Department, Faculty of Medicine, Banha University, Benha, Egypt, **Tel.:** +20 1097390300, **E-mail:** heba.bayoumi@fmed.bu.edu.eg

ISSN: 1110-0559, Vol. 43, No.2

INTRODUCTION

Diabetes mellitus (DM) is one of the most prevailing non-communicable, metabolic disorder characterized by hyperglycemia resulting from defective insulin production, resistance to insulin action or both. Prolonged exposure to chronic hyperglycemia can lead to many ailments including both vascular and nonvascular complications^[1]. Diabetic retinopathy (DR) is a microvascular disease associated with chronic inflammation and retinal neurodegeneration, which is influenced by local, systemic, metabolic and cardiovascular parameters. It involves microvascular changes as well as changes in the all main cell types of the retina. Degeneration, inflammation and vascular alternations occur and operate parallel and in close relation^[2].

Current DR therapeutic strategies may include laser photocoagulation vitreoretinal surgery, and intravitreal injection of vascular endothelial growth factor (VEGF) neutralizing agents (e.g., ranibizumab) or corticosteroids,

but these therapies have achieved only limited success^[3]. No treatment has yet been developed to support regeneration of the damaged retinal vasculature as a result of long-term hyperglycemia. Cell-based therapies may be an achievable option for both preventing neurovascular damage and promoting regeneration of damaged retina^[4].

Cell therapy can be defined as a set of strategies which use live cells with therapeutic purposes. The aim of such therapy is to repair, replace or restore the biological function of a damaged tissue or organ. Thus, the use of stem cells in cell therapy is being studied in numerous areas of medicine^[5]. These therapies include embryonic stem cells (ESCs), induced pluripotent stem cells (iPSCs), mesenchymal stem cells (MSCs), adipose stem cells (ASCs) and retinal progenitor cells (RPCs), as well as RPE replacement^[6]. It is accepted that MSCs function in a paracrine manner in vivo and not by direct differentiation. In addition to soluble factors, exosomes are now supposed to be important mediators for the paracrine effect of MSCs and possess similar functions to MSCs^[7].

The main challenges of cell replacement therapy include; the delivery and integration of regenerative materials to the eye, overcoming the opportunity of immune rejection and the guidance of neural growth to establish functional connections^[6].

Exosomes are extracellular vesicles which range in size from 40 to 150 nm and generated by fusion of multivesicular bodies (MVBs) with plasma membrane^[8]. They are released by several types of cells, including mast cells, dendritic cells, B lymphocytes, neurons, adipocytes, endothelial cells, epithelial cells and mesenchymal cells^[9]. Exosomes have recently come into focus of research based on their high capacity to interact with target cells and their ability to selectively modify cell signaling^[10].

The aim of this study was to evaluate the efficacy of bone marrow mesenchymal stem cell and their exosomes in treatment of induced DR in adult albino rats.

MATERIAL AND METHODS

Drugs and Chemicals

Streptozotocin was purchased in a white powder (Sigma Chemical Co., St. Louis, USA). It was given as single intraperitoneal (IP) injection of freshly prepared STZ (60 mg/kg, dissolved in 0.1 M cold citrate buffer, pH 4.5) for each rat^[11].

Bone Marrow Mesenchymal Stem Cells

The BMMSCs were prepared in Stem cell unit, Central lab, Benha Faculty of Medicine, and injected intravitreally in a dose of 0.2ml solution containing 200×103 BMMSCs for each rat^[12].

MSCs Derived Exosomes Labelled with PKH26

Exosomes were prepared in the stem cell and molecular biology unit, central lab, Cairo faculty of medicine. BMMSCs-exosomes were isolated from conditioned media of rat bone marrow derived MSC. They were labelled by fluorescent dye PKH26 and injected intravitreally in single dose of 0.5 ml for each rat at concentration (100 µg protein /mL)^[7].

Animals and Diet

Sixty-four healthy adult male albino rats of weight range 250-300 grams for each were utilized in this study. Another ten young rats were used to prepare the BMMSCs. The rats were obtained from the animal house, Moshtohor Faculty of Veterinary Medicine, Benha University. The animals were housed in special cages and fed with adequate available tap water and commercial diet. All Benha faculty of medicine ethical protocols for animal treatment were followed. The animal experimental protocol received approval from Institutional Animal Care Committee. Animal care was provided by laboratory animal house in pharmacology department, Benha faculty of medicine.

Experimental Design

After one week of acclimatization, 64 adult rats were randomly divided into six groups:

Group I (control group; n= 24): The rats were divided equally into three subgroups: subgroup Ia: The rats were left without intervention. Subgroup Ib: The rats were injected intraperitoneally with a single dose of 0.2 mL/kg body weight sodium citrate buffer (vehicle for STZ) Subgroup Ic: Rats were received single intravitreal injection of 0.2 ml phosphate buffer saline (vehicle for Stem Cells and exosomes).

Group II (affected group; n= 8): Each rat received single intraperitoneal (IP) injection of freshly prepared STZ (60 mg/kg, dissolved in 0.1 M cold citrate buffer, pH 4.5). Diabetic rats received long-acting insulin (2–4 U/rat) through subcutaneous injection to keep blood glucose levels in a desirable range (350 mg/dL).

Group III (DR + Stem Cells; n= 8): Rats treated as group II, then 8 weeks after induction of diabetes, rats were injected intravitreally with single dose of 0.2ml solution containing 200×103 BMMSCs for each rat.

Group IV (DR + exosomes; n=8): Rats treated as group II, then 8 weeks after induction of diabetes rats were injected intravitreally with MSC-exosomes in single dose of 0.5 ml for each rat at concentration (100 µg protein /mL).

Group V (DR + Stem Cells + exosomes; n=8): Rats treated as group II, then 8 weeks after induction of diabetes rats were injected once with BMMSCs and MSC-exosomes together intravitreally in the same doses as group III and IV.

Group VI (Recovery group; n=8): Rats treated as group II.

At the end of the 8th week, rats of group II were sacrificed, while rats of other groups were sacrificed at the end of 12th week after induction of diabetes. Rats were anesthetized by ether and sacrificed by cervical decapitation, then both eyeballs were enucleated from rats of all groups.

Induction of Diabetes Mellites Type I Rat Model

Type I diabetes mellitus (DM) was produced according to the process illustrated by some authors^[11]. DM was induced in overnight fasted rats by injection of single intraperitoneal (IP) injection of freshly prepared STZ (60 mg/kg, dissolved in 0.1 M cold citrate buffer, pH 4.5) for each rat. After STZ injection, rats acquired drinking water containing sucrose (15 g/L) for 48 h, to reduce the early death due to insulin discharge from partially injured pancreatic islets. Seventy-two hours later, rats were checked for hyperglycemia, and those with fasting blood sugar more than 250 mg/dL were included in the study. Diabetic rats received long-acting insulin

(2–4 U/rat) through subcutaneous injection to keep blood glucose levels in a desirable range (350 mg/dL) and to avoid consequent development of ketonuria.

Isolation and Characterization of BMSC^[13]

BM was harvested by flushing the tibiae and femora of 6-week-old male Sprague-Dawley albino rats with Dulbecco's modified Eagle's medium supplemented with 10% fetal bovine serum. Nucleated cells were isolated and resuspended in complete culture medium supplemented with 1% penicillin–streptomycin. The cells were incubated at 37°C in 5% humidified CO₂ for 12–14 days as primary culture or upon formation of large colonies. When they developed (80–90% confluence), the cultures were washed twice with PBS and the cells were trypsinized with 0.25% trypsin in 1 mmol/l EDTA for 5 min at 37°C. After centrifugation, the cells were resuspended in serum-supplemented medium and incubated in a culture flask. The resulting culture was referred to as first-passage culture. BM-MSCs in culture were characterized by their adhesiveness and fusiform shape under a phase-contrast microscope^[11]. All cultures were examined using an inverted microscope; Leica DM IL LED with camera Leica DFC295 (Leica Microsystems CMS GmbH, Ernst-Leitz-Straße 17-37, Wetzlar, D-35578, Germany).

Flow cytometric analysis^[14]

Analysis of cell surface molecules (CD34 and CD45), representing the hematopoietic markers, and (CD90 and CD105), representing the mesenchymal stem cell markers was performed on cultured stem cells after being detached and suspended in PBS. On the day of analysis, unattached cells in cultures were washed out with PBS, and adherent cells were trypsinized. After washing, cells were suspended in 0.5% BSA in PBS at a concentration of 4x10⁴ per mL and incubated in blocking buffer (containing 25 µg/mL IgG) for 10 min followed by 40-min incubation with antibodies labeled with fluorescein isothiocyanate (FITC) against CD34, CD45, CD90 and antibodies labeled with phycoerythrin (PE) (Beckman Coulter, France) against CD105 and acquired onto FACS Calibur (Beckman Coulter, NE15106, USA).

Preparation of MSCs-Derived Exosomes (MSCs-exosomes)^[15]

MSC-derived exosomes were obtained from the supernatant of MSCs, representing conditioned media. The MSCs were cultured in Dulbecco's Modified Eagle Medium (DMEM) without fetal bovine serum (FBS), but with 0.5% human serum albumin (HSA) (Sigma-Aldrich, St. Louis, MO, USA), overnight. The viability of the cells cultured overnight was more than 99%, as detected by trypan blue exclusion. Cells were plated at 4000 cells/cm² for 7 days. On day 7, cells were trypsinized, counted, and replated in expansion medium at a density of 2000 cells/cm² for another seven days (end of passage 1). The expansion was performed until the third passage. The conditioned medium was collected and stored at –80 °C. The medium

was centrifuged at 2000g for 20 min to remove debris, and then ultracentrifuged at 100,000× g in a SW41 swing rotor (Beckman Coulter, Fullerton, CA, USA) for 1 hour at 4 °C. Exosomes were washed once with serum-free M199 (Sigma-Aldrich) containing 25 mM 4-(2-hydroxyethyl)-1-piperazineethanesulfonic acid (HEPES) (pH = 7.4), and submitted to a second ultracentrifugation in the same conditions. Exosomes were labeled with PKH26 fluorescent linker dye to trace them *in vivo*. Exosomes were stored at –80 °C for the experiment.

Exosome Labeling with PKH-26^[16]

PKH26 (Sigma-Aldrich, St. Louis, MO, USA) was used to confirm the exosome localization within the retinal tissue. The exosome pellet was diluted with PKH-26 kit solution to 1 mL, and 2 µL of fluorochrome was added to this suspension and incubated at 38.5 °C for 15 min. After that, 7 mL of serum-free HG-DMEM (high glucose-modified eagles medium was added to the suspension, then it was ultracentrifuged for second time at 100,000× g for 1 h at 4 °C. The final pellet was resuspended rapidly in HG-DMEM and stored at –80 °C for future injection in experimentally induced rats. Fluorescent-labeled MSCs-EX were detected in retinal cryosections using fluorescence microscope (Leica Microsystems CMS GmbH, Wetzlar, Germany).

Histological and Immunohistochemical Studies

paraffin sections of 5–7 µm thickness, mounted on glass slides for Hematoxylin and Eosin stain^[17] to examine the histological changes in the different groups. Other sections were mounted on +ve charged slides for immunohistochemical staining:

1. Immunohistochemical staining for detection of VEGF (index for angiogenesis). The primary monoclonal antibody used was the goat polyclonal antibody (Santa Cruz Company, California, USA) (1:500 with PBS). The cellular site of the reaction was cytoplasmic brown in color^[18].
2. Immunohistochemical staining for detection of vimentin (index for gliosis). The primary monoclonal antibody used was the Vimentin mouse monoclonal antibody (Santa Cruz Biotechnology, Santa Cruz, California, USA) (1:300 wit PBS). The cellular site of the reaction was cytoplasmic brown in color^[19].
3. Immunohistochemical staining for detection of CD105 (surface marker of MSCs) the Primary Antibody was Ab-1 monoclonal antibody, Clone QBEnd/10, Lab Vision Corporation laboratories, CA 94539, USA^[20].

Immunohistochemical study was conducted using the avidin–biotin peroxidase method, followed by diaminobenzidine (DAB) (Dakopatts, Glostrup, Denmark) was added to slides as a chromogen). Thereafter, the slides were washed with distilled water. Later, the sections were counterstained with hematoxylin.

Transmission Electron Microscope (TEM) of MSCs-EXOS^[21]

Exosomes were gently placed on Formvar-coated copper grids. They were allowed to be adsorbed for 45 min and then handled for standard uranyl acetate staining. The grids were irrigated with PBS three times and left to semidry at room temperature prior to examining in TEM. Images were obtained by using TEM JEOL (JEM-2100; Akishima, Tokyo, Japan) at an accelerating voltage of 80 kV.

Transmission Electron Microscopic (TEM) study^[22]

Ultrathin sections were prepared in Tanta EM Unit, Faculty of Medicine, Tanta University, Tanta, Egypt. Grids were examined and electron micrographs were taken using transmission electron microscope JOEL (JEM-100 SX, Akishima, Tokyo, Japan) in, Electron Microscope unit, Tanta faculty of medicine, Tanta University.

Morphometric Study and Statistical Analysis

Eight slides from different rats of each group (n=8) were assessed. The mean area percentage of positive immunorexpression of VEGF and vimentin was assessed in 10 nonoverlapping fields of each section at x400 magnification using Image-Pro Plus program version 6.0 (Media Cybernetics Inc., Bethesda, Maryland, USA). Data was analyzed using Statistical Package for Social Science software computer program version 23 (SPSS, Inc., Chicago, IL, USA). Data were presented in mean and standard deviation. Oneway Analysis of variance (ANOVA) followed by post-hoc and tukey was used for comparing different groups. *P value* less than 0.05 was considered statistically significant.

RESULTS

BMMSCs Characterization and Tracking

MSCs were identified in culture by inverted microscope as adherent spindle shaped cells between rounded cells at day 14 of culture (Figure 1). BMMSCs were identified by flow cytometric analysis showing that they are positive for CD 90 and CD105 additionally, they negative for CD34 and CD45 (Figure 2). MSCs were detected in the retinal tissues by CD105 immunohistochemical study (Figure 3).

MSCs-Exosomes Characterization

A transmission electron microscopy examination of purified exosomes demonstrated by their characteristic spheroid double-membrane bound morphology with a diameter of 90-100 nm (Figure 4a). Exosomes labelled with PKH26 fluorescent dye were detected in retinal tissues as strong red fluorescence (Figure 4b).

H & E Results

Examination of all subgroups of the control group showed similar histological architecture. Group I (control group) showed normal retina consists of ten layers from outward to inward; retinal pigment epithelial (RPE) layer,

photoreceptor layer (PRL), outer limiting membrane (OLM), outer nuclear layer (ONL), outer plexiform layer (OPL), inner nuclear layer (INL), inner plexiform layer (IPL), ganglionic cell layer (GCL), nerve fiber layer (NFL) and inner limiting membrane (ILM) (Figure 5).

Group II (affected group) showed apparent decrease of retinal thickness. GCL revealed ganglion cells (GC) with wide clear areas around shrunken nuclei and large dilated congested blood vessels. The inner nuclear layer (INL) displayed small nuclei, focal widening of intercellular spaces and multiple congested blood vessels encroaching toward the outer plexiform layer (OPL). Focal widening of intercellular spaces in the ONL were also seen (Figure 6).

Group III (DR + SC) showed some ganglionic cells nuclei were shrunken with slightly diminished clear areas. New blood vessels in the inner nuclear layer were encroaching toward the outer plexiform layer. Focal widening of intercellular spaces between the cells of the outer nuclear layer. Blood telangiectasias indicating new vessel formation (Figure 7).

Group IV (DR + Exosomes) showed apparently increased retinal thickness, with more regularly arranged layers. Small blood vessels were seen in the inner nuclear layer and the outer plexiform layer (Figure 8).

Group V (DR + SC+ Exosomes) showed nearly normal retinal histological architecture. Ganglion cells appear with vesicular nuclei and small blood vessel was seen in the outer plexiform layer (Figure 9).

Group VI (Recovery group) showed apparent marked reduction in the retinal thickness. The GCL revealed pyknotic nuclei of ganglionic cells with some vacuolation. The nuclei of the inner nuclear layer (INL) and outer nuclear layer (ONL) are small and darkly stained. Multiple dilated new blood vessel in the nerve fiber layer (NFL) and the ganglion cell layer (GCL). Widening of intercellular spaces between the cells of the outer nuclear layer (ONL). The choriocapillaris layer had dilated congested blood vessels (Figure 10).

VEGF Staining Results

Group I showed negative immunoreaction for vascular endothelial growth factor (VEGF) in almost all retinal layers (Figure 11). Group II showed markedly positive immunoreaction for VEGF especially in nerve fiber layer, ganglion cell layer and outer plexiform layer (Figure 12). Group III showed moderate positive VEGF immunoreaction in NFL, GCL and OPL of retina (Figure 13). Group IV showed mild positive VEGF immunoreaction in NFL and OPL of retina (Figure 14). Group V showed minimal positive VEGF immunoreaction in GCL and INL of retina (Figure 15). Group VI showed intense positive VEGF immunostaining in NFL, GCL and OPL of retina (Figure 16).

Vimentin Staining Results

Group I showed minimal vimentin immunoreactivity in the Muller cell end feet at the inner limiting membrane

(ILM). Positively stained fine brown Muller's radial processes appear as long filaments extending in NFL, GCL, IPL, INL, OPL and ONL (Figure 17). Group II showed markedly positive vimentin immunostaining of muller cell bodies and their processes and observed throughout most retinal layers (Figure 18). Group III showed moderate positive vimentin immunostaining of muller cell bodies and their processes (Figure 19). Group IV showed mild positive vimentin immunostaining of muller cell bodies and their processes (Figure 20). Group V showed little positive vimentin immunostaining of muller cell bodies and their processes (Figure 21). Group VI showed intense positive vimentin immunostaining of muller cell bodies and their processes observed throughout most retinal layers especially in the NFL and GCL (Figure 22).

EM Results

Retinal Pigment Epithelium and Photoreceptor outer segment:

Group I showed Retinal Pigment Epithelial (RPE) cells and photoreceptors outer segments (POS). RPE was resting on Bruch's membrane with large euchromatic oval nucleus, basal mitochondria and long apical microvilli surrounding the outer segment of the photoreceptor. POS appeared as elongated, straight structures. Parallel lamellar structures of the outer segment of photoreceptors and Choriocapillaris layer could be noticed (Figure 23).

Group II showed retinal pigmented cells with extensively destructed broken apical microvilli, karyolytic nucleus, and numerous large phagosomes. The photoreceptor outer segments were markedly disorganized and vacuolated with loss of normal orientation of their lamellar disc membranes. There were wide areas of complete loss of photoreceptors outer segments (Figure 24).

Group III showed retinal pigmented cells resting on distorted Bruch's membrane and had large oval nuclei with some broken apical microvilli. Multiple photoreceptor outer segments were present. Some of them were with normal lamellar appearance and others with loss of normal orientation of their lamellar disc membranes and still showing vacuolations. There were areas of loss of photoreceptors outer segments (Figure 25).

Group IV showed retinal pigmented epithelial cells resting on Bruch's membrane with oval large heterochromatic nuclei and apical microvilli. Multiple photoreceptor outer segments were slightly separated by spaces. Some of these segments were with normal lamellar appearance, and others had vacuolation (Figure 26).

Group V showed nearly normal Retinal pigment epithelium resting on Bruch's membrane separating it from the Choriocapillaris layer. RPE had large oval heterochromatic nuclei and many long apical microvilli enclosing the outer segments. The photoreceptors outer segments were with lamellar membranous discs (Figure 27).

Group VI showed retinal pigmented cells with shrunken nuclei that had areas of heterochromatin, vacuolated cytoplasm, distorted apical microvilli, and large phagosomes. The photoreceptor outer segments were markedly distorted and shrunken. There were large spaces filled with debris. Protruded some photoreceptors nuclei into the area of the outer segments could be seen (Figure 28).

Outer nuclear layer (ONL)

Group I showed outer nuclear layer with predominate rod cells. Their nuclei were more rounded, heterochromatic with highly condensed centrally located chromatin, and were surrounded by a thin rim of cytoplasm. The cells were tightly backed with no intercellular spaces. Outer plexiform layer could be seen, with many processes containing mitochondria (Figure 29).

Group II showed degenerated cells with severe cytoplasmic vacuolization. The cells were separated by intercellular spaces filled with debris. Pyknotic nuclei could be seen (Figure 30).

Group III showed many photoreceptor nuclei with heterochromatin. Wide areas separating the photoreceptor nuclei and many cytoplasmic vacuolations were noticed (Figure 31).

Group IV showed many photoreceptor nuclei with heterochromatin. little intercellular spaces were separating the cells (Figure 32).

Group V showed nearly normal nuclei with heterochromatin surrounded by rim of cytoplasm, with no intercellular spaces between the cells. Processes of muller cell can be noticed with electron lucent cytoplasm and different organelles (Figure 33).

Group VI showed apparently decreased number of photoreceptor cells nuclei and many degenerated cells with severe cytoplasmic vacuolization. Some areas showed complete degeneration of photoreceptor nuclei and were filled with debris. Some other pyknotic nuclei were present (Figure 34).

Inner nuclear layer (INL)

Group I showed amacrine cells with large, pale euchromatic nuclei. Müller cells have dense nuclei and irregular outlines with prominent processes. The cell bodies of bipolar cells containing round nuclei. Normal retinal blood capillaries lined with endothelial cell could be observed (Figure 35).

Group II showed many cytoplasmic vacuolation and mitochondria with destructed cristae in inner nuclear layer cells. Some amacrine cells had disintegrated cytoplasm filled with rough endoplasmic reticulum. Another amacrine cells showed large nuclei with heterochromatin. Bipolar cells showed shrunken nuclei with much peripheral heterochromatin (Figure 36).

Group III showed amacrine cells had irregular shrunken nuclei with peripheral heterochromatin and their cytoplasm showed mitochondria with destructed cristae. The nuclei of some bipolar cells appeared irregular with dense areas. Few Müller cells showed large irregular nuclei with dilated perinuclear membrane and phagocytic dense bodies (Figure 37).

Group IV showed few amacrine cells had shrunken nuclei with areas of peripheral heterochromatin. Some Müller cells appeared irregular in shape with dark irregular nuclei and dilated nuclear envelope. Other Müller cells showed shrunken nuclei with indentations, dilated rough endoplasmic reticulum and slight mitochondria with destructed cristae could be detected. The other amacrine and bipolar cells appeared nearly normal (Figure 38).

Group V showed nearly normal Müller, amacrine and bipolar cells. Few bipolar cells revealed mitochondrial destructed cristae. Müller cells appeared with prominent processes (Figure 39).

Group VI showed degenerated amacrine and bipolar cells with decrease in the cell density. The degenerated cells were at various stages of disintegration and most of their cytoplasmic organelles were absent. The empty spaces left by degenerated cell bodies and processes were filled with debris. Müller cells appeared with irregular thin cytoplasmic processes (Figure 40).

Ganglion cell layer (GCL)

Group I showed ganglion cells had large rounded euchromatic nuclei with uniformly staining nucleoplasm and prominent nucleoli. Few mitochondria, Rough endoplasmic reticulum and scattered ribosomes were observed. Ganglion cells axons developed from a portion of the axon hillock were observed (Figure 41).

Group II showed degenerated ganglion cells with indented nuclei exhibiting highly convoluted sinuses and areas of electron-dense heterochromatin. Swollen mitochondria with destructed cristae and decreased matrix density could be noticed. The cytoplasm revealed vacuolation (Figure 42).

Group III showed ganglion cells with oval nuclei and swollen mitochondria with destructed cristae (Figure 43).

Group IV showed ganglion cells with large euchromatic nuclei. Some mitochondria appeared swollen with destructed cristae (Figure 44).

Group V showed nearly normal ganglion cells with large oval euchromatic nuclei. The cytoplasm contains plenty of ribosomes, slightly dilated RER and slightly swollen mitochondria. Ganglion cells axons developed from a portion of the axon hillock (Figure 45).

Group VI showed ganglion cells with highly rarefied cytoplasm containing large vacuoles. Nuclei showing vacuolation with slightly dilated nuclear envelope. Area of disrupted envelope could be noticed. The inner limiting membrane appeared abnormal and the inner plexiform layer showed destructed axons (Figure 46).

Morphometric and Statistical Results

The mean area percentage \pm SD of VEGF and vimentin immunostaining are represented in Tables and (Histograms 1&2). The mean area percentage of VEGF and vimentin we significantly increased ($P<0.05$) in groups II and VI compared with group I. The mean area percentage of VEGF and vimentin we significantly decreased ($P<0.05$) in groups III, IV&V compared with group II. The mean area percentage of VEGF and vimentin were significantly decreased ($P<0.05$) in group V compared to groups III&IV.

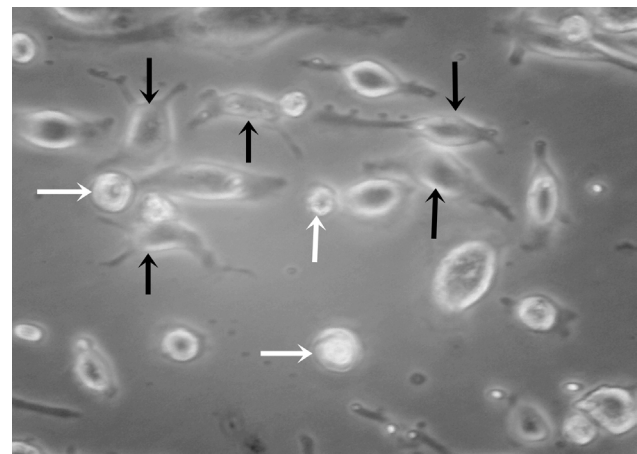


Fig. 1: An inverted microscope micrograph on day 14 from primary culture of MSCs showing adherent spindle shaped cells (black \uparrow) between rounded non adherent cells (white \uparrow). (X400)

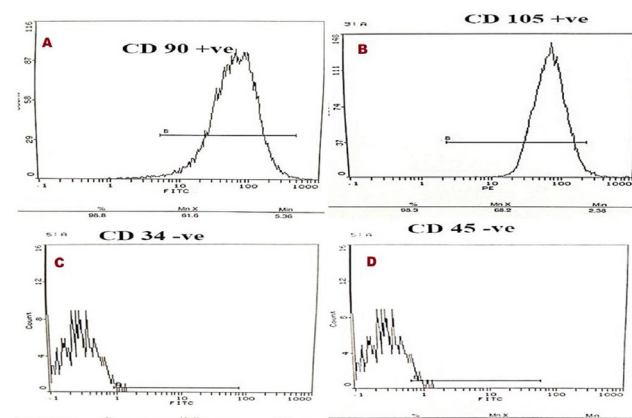


Fig. 2: Flow cytometric analysis images of MSCs showing that they are: (A) positive for CD90 (98.8%). (B) positive for CD105 (98.3%). (C) negative for CD 34 (1.11%). (D) negative for CD 45 (4.73%).

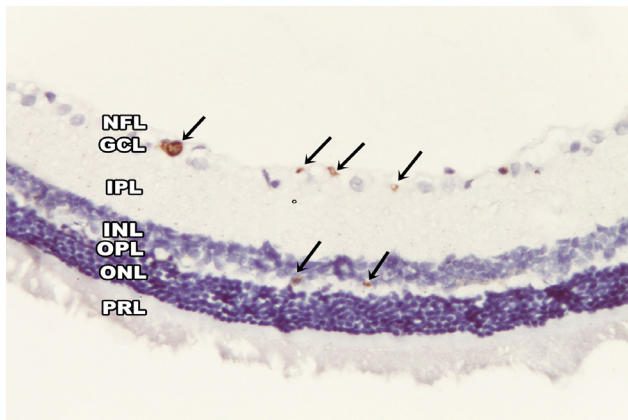


Fig. 3: A photomicrograph of a section in rat retina of group III (DR injected with stem cells) showing positive CD105 expression (arrow) in the outer plexiform layer (OPL), inner nuclear layer (INL) and ganglion cell layer (GCL). (CD 105 immunostaining X 400)

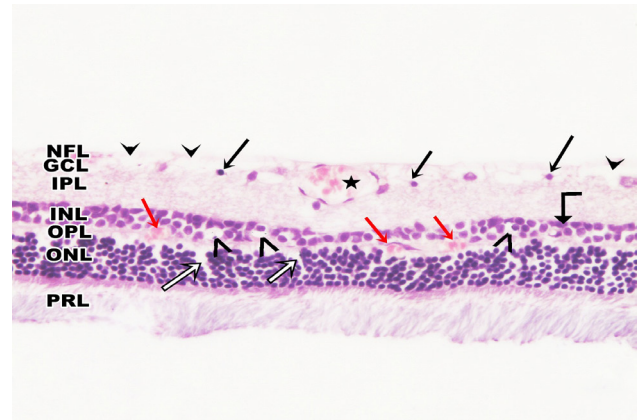


Fig. 6: A photomicrograph of a section in the retina of group II (affected group) showing apparent decrease of retinal thickness. The GCL revealed shrunken nuclei (black arrow) and wide clear areas (arrow heads). Focal widening of intercellular spaces of the inner nuclear layer (>) and the outer nuclear layer (white arrow). The nuclei of the INL appear small and darkly stained (angled arrow). large dilated congested blood vessel appeared in GCL (*). Multiple congested blood vessels (red arrows) in the inner nuclear layer (INL) encroaching toward the outer plexiform layer (OPL). (X400)

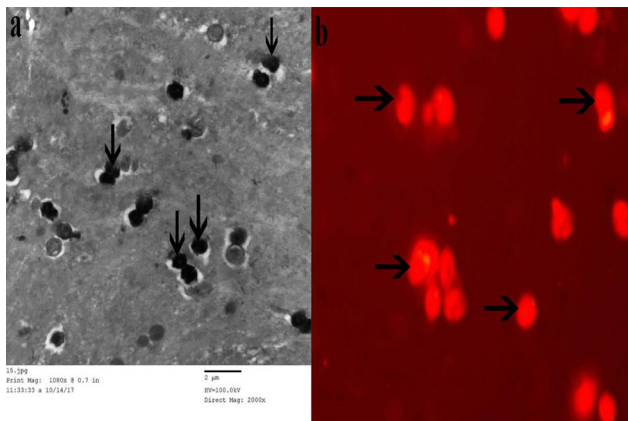


Fig. 4: (a) A transmission electron micrograph of exosomes demonstrated their characteristic spheroid double-membrane bound morphology with a diameter of 90-100 nm (black ↑). (b) A fluorescent microscope photograph showing homing of exosomes labelled with PKH26 dye in retinal tissue (arrow). (X1000)

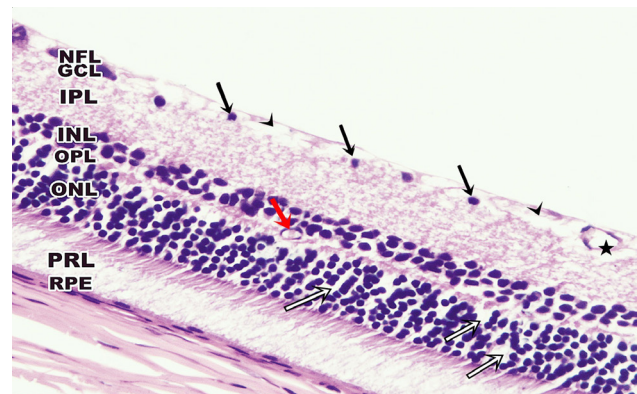


Fig. 7: A photomicrograph of a section in the retina of group III (DR +SC) showing the GCL with shrunken darkly stained nuclei (black ↑) of some ganglionic cells and clear areas (arrow head). Blood vessel in the GCL (*) and in the INL (red ↑) encroaching toward the outer plexiform layer. Focal widening of intercellular spaces between the cells of the ONL (white ↑). (X400)

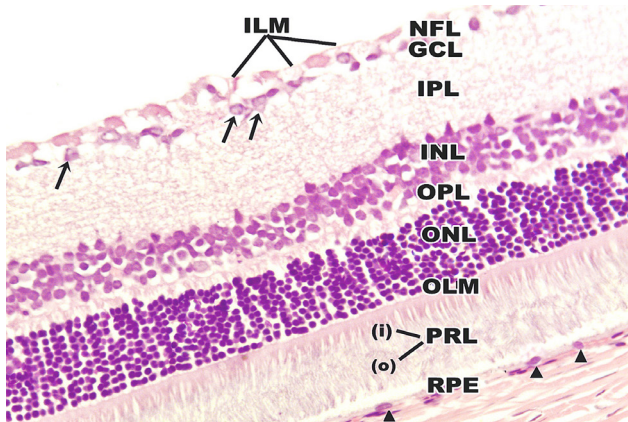


Fig. 5: A photomicrograph of a section in the retina of group I (control group) showing the normal retina consists of 10 layers from outward to inward; Retinal pigment epithelium (RPE) single layer of cells with oval nuclei (▲), the photoreceptor layer (PRL) with outer segments (o) and inner segments (i) of rods and cones, the outer limiting membrane (OLM), the outer nuclear layer (ONL), the outer plexiform layer (OPL), the inner nuclear layer (INL), the inner plexiform (IPL), the ganglion cell layer (GCL) with large vesicular nuclei (arrows), the nerve fiber layer (NFL) and the inner limiting membrane (ILM). (X400)

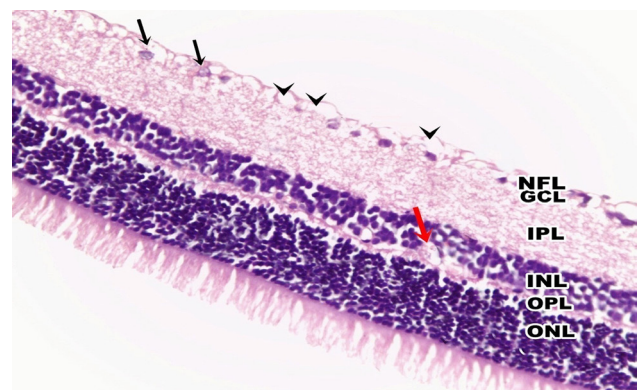


Fig. 8: A photomicrograph of a section in the retina of group IV (DR + Exosomes) showing apparently increased retinal thickness, with more regularly arranged layers. Some ganglionic cells appear with euchromatic nuclei (black ↑), with slightly decreased intercellular spaces between the cells (arrow head). Small blood vessel (red ↑) can be seen in the inner nuclear layer (INL) and outer plexiform layer (OPL). (X400)

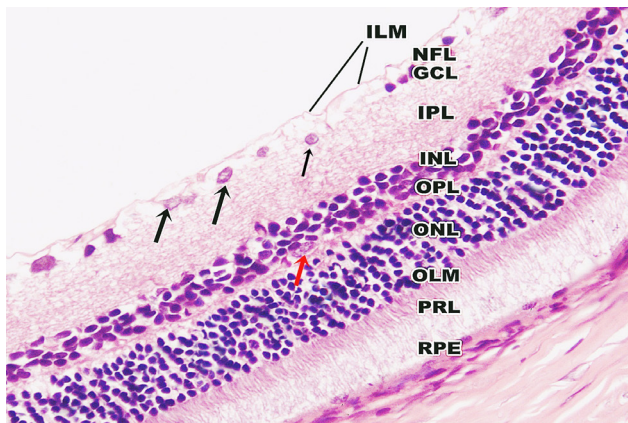


Fig. 9: A photomicrograph of a section in the retina of group V (DR + SC+ Exosomes) showing nearly normal histological architecture. Ganglion cells showing vesicular nuclei (black ↑). Small blood vessel (red ↑) can be seen in the outer plexiform layer (OPL). (X400)

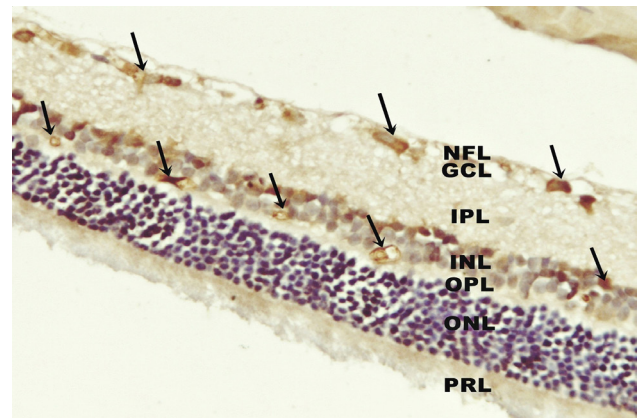


Fig. 12: A photomicrograph of a section in the retina of group II (affected group) showing markedly positive VEGF immunoreaction (arrow) especially in NFL, GCL and OPL. (Anti-VEGF immunostaining, ×400)

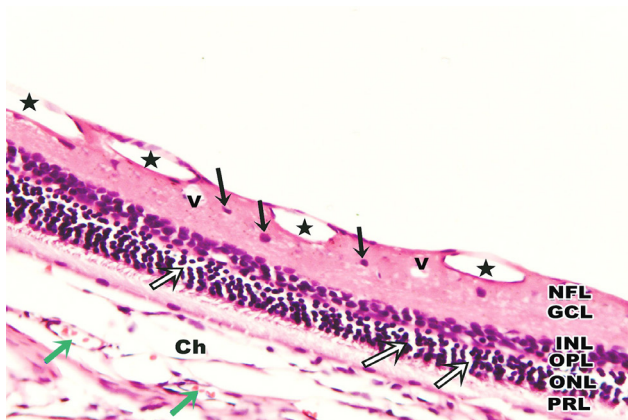


Fig. 10: A photomicrograph of a section in the retina of group VI (recovery group) showing apparent marked reduction in retinal thickness. The GCL revealed shrunken pyknotic nuclei (black ↑) of ganglion cells with some vacuolation (v). The nuclei of the inner nuclear layer (INL) and outer nuclear layer (ONL) are small and darkly stained. Multiple dilated blood vessels (star) in the nerve fiber layer (NFL) and ganglion cell layer (GCL). Widening of intercellular spaces (white arrow) between the cells of the outer nuclear layer (ONL). Part of the choriocapillary layer (Ch) can be seen with dilated congested blood vessels (green arrow). (X400)

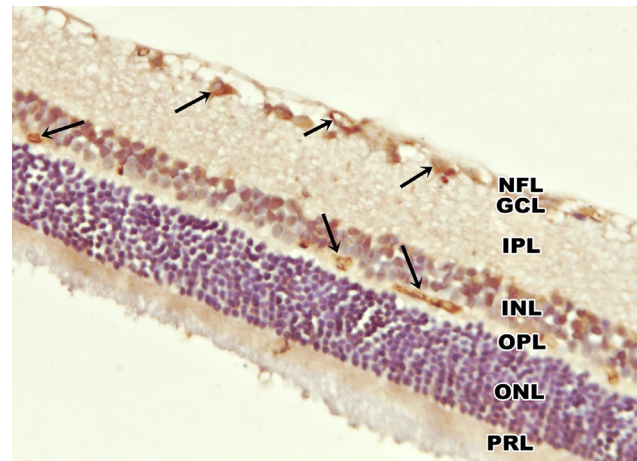


Fig. 13: A photomicrograph of a section in the retina of group III (DR + SC) showing moderate positive cytoplasmic immunoreaction (arrow) in NFL, GCL and OPL of the retina. (Anti-VEGF immunostaining, ×400)

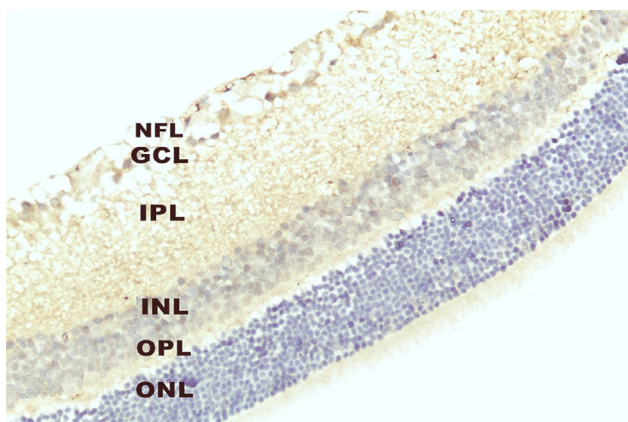


Fig. 11: A photomicrograph of a section in the retina of group I (control group) showing negative immunoreaction for vascular endothelial growth factor (VEGF) in almost all retinal layers. (Anti-VEGF immunostaining, ×400)

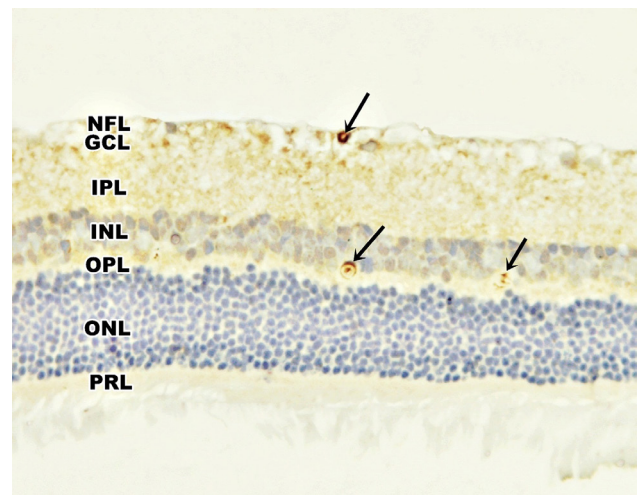


Fig. 14: A photomicrograph of a section in the retina of group IV (DR + Exosomes) showing mild positive immunoreaction (arrow) for vascular endothelial growth factor (VEGF) in many layers of the retina. (Anti-VEGF immunostaining, ×400)

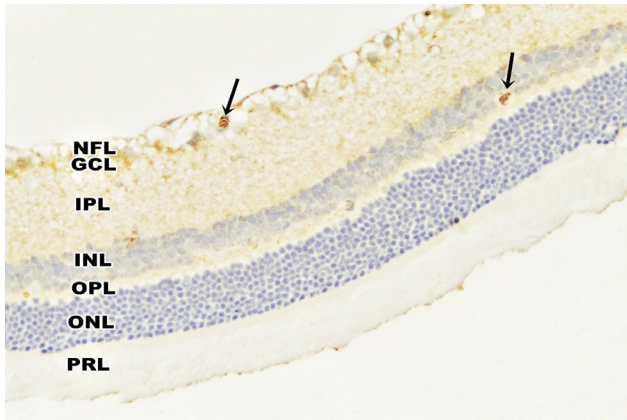


Fig. 15: A photomicrograph of a section in the retina of group V (DR + SC + Exosomes) showing minimal positive VEGF immunoreaction (arrow) in GCL and INL of retina. (Anti-VEGF immunostaining, ×400)

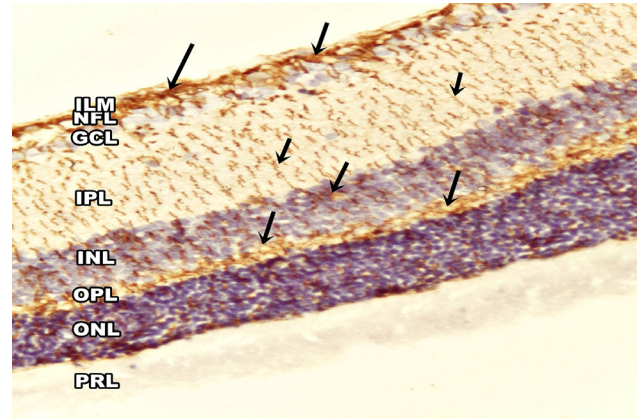


Fig. 18: A photomicrograph of a section in the retina of group II (affected group) showing marked vimentin immunostaining of muller cell bodies and their processes. (Anti-Vimentin immunostaining, ×400)

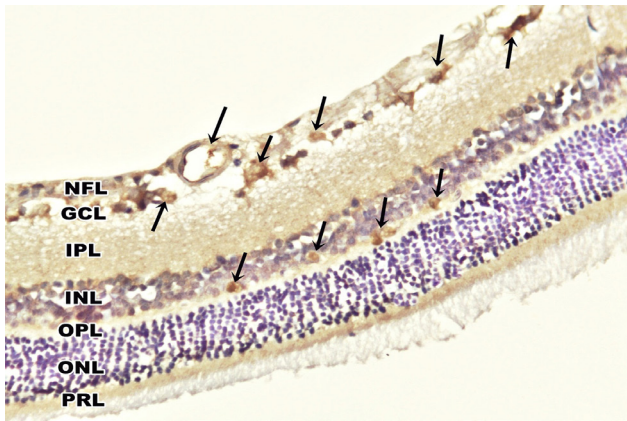


Fig. 16: A photomicrograph of a section in the retina of group VI (recovery group) showing intense positive VEGF immunoreaction (arrow) in NFL, GCL and OPL of retina. (Anti-VEGF immunostaining, ×400)



Fig. 19: A photomicrograph of a section in the retina of the group III (DR + SC) showing moderate positive vimentin immunostaining of muller cell bodies and their processes in NFL, INL, OPL and ONL (arrows). (Anti-Vimentin immunostaining, ×400)

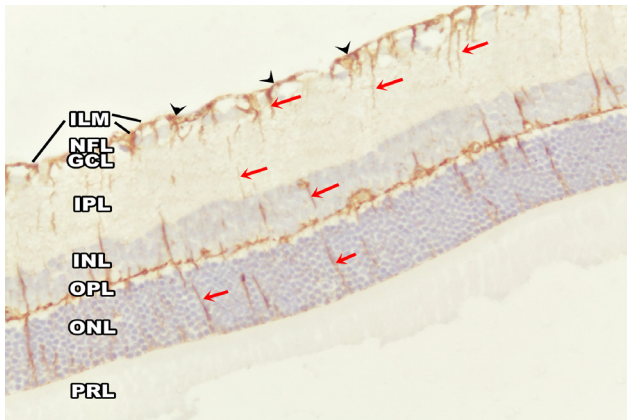


Fig. 17: A photomicrograph of a section in the retina of group I (control group) showing minimal vimentin immunostaining in the Muller cell end feet (arrow head) at the inner limiting membrane (ILM). Positively stained fine brown Muller's radial processes appear as long filaments (red arrow) extending in NFL, GCL, IPL, INL, OPL and ONL. (Anti-Vimentin immunostaining, ×400)

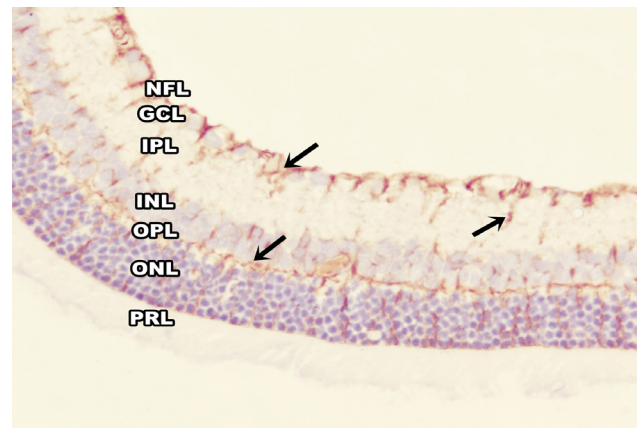


Fig. 20: A photomicrograph of a section in the retina of the group IV (DR + Exosomes) showing mild positive vimentin immunostaining of muller cell bodies and their processes in NFL, IPL, INL and OPL (arrows). (Anti-Vimentin immunostaining, ×400)

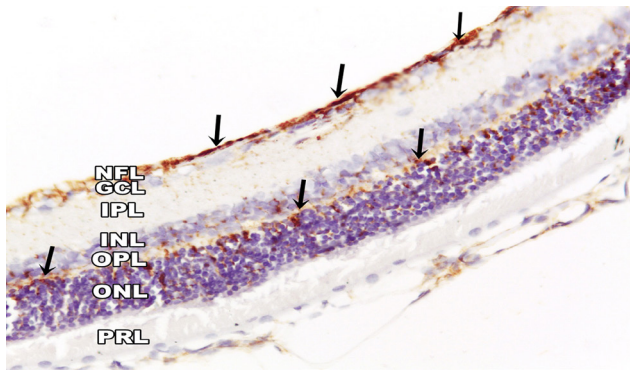


Fig. 21: photomicrograph of a section in the retina of the group V (DR + SC + Exosomes) showing little positive vimentin immunostaining of muller cell bodies and their processes in NFL and OPL (arrows). (Anti-Vimentin immunostaining, $\times 400$)

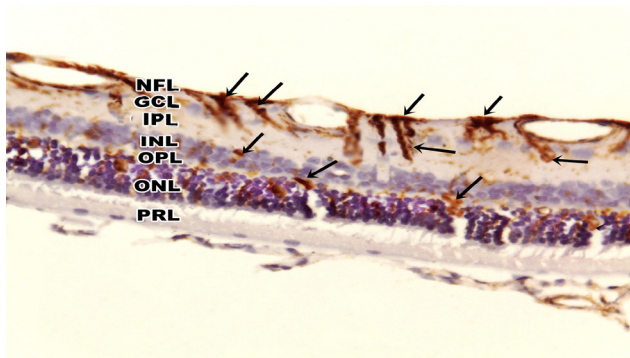


Fig. 22: A photomicrograph of a section in the retina of the group VI (recovery group) showing intense positive vimentin immunostaining of muller cell bodies and their processes observed throughout most retinal layers (arrows) especially in the NFL, GCL, IPL and OPL. (Anti-Vimentin immunostaining, $\times 400$)

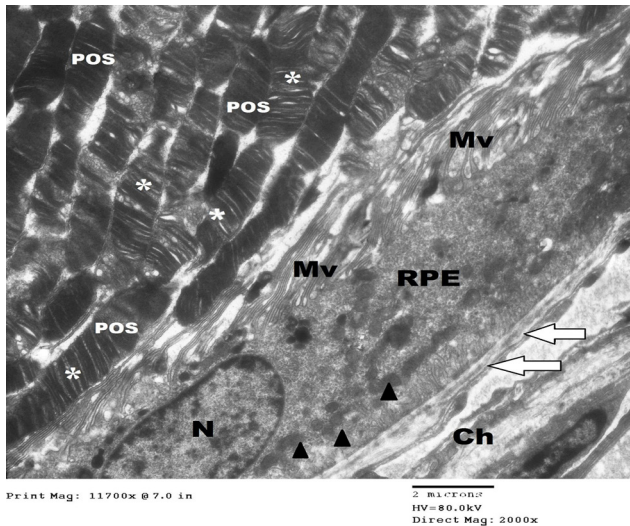
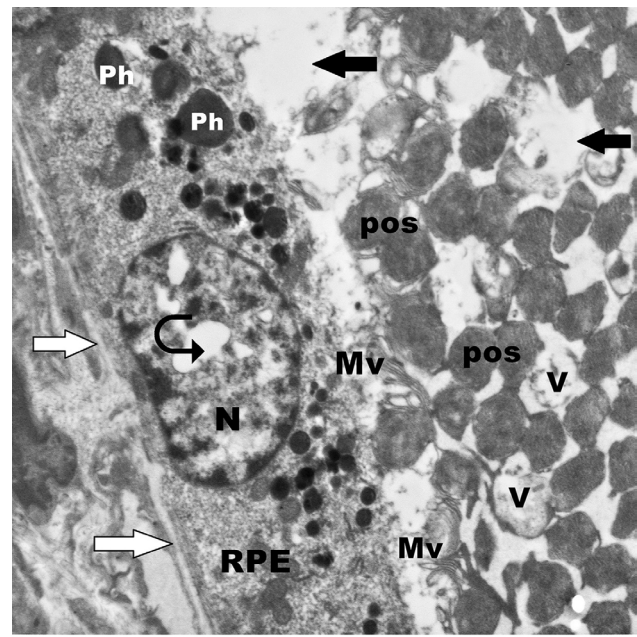


Fig. 23: A transmission electron micrograph of a section in the retina of group I (control group) showing a part of retinal pigment epithelial (RPE) cell and some photoreceptors outer segments (POS). RPE is resting on Bruch's membrane (thick white arrow) with large euchromatic oval nucleus(N), basal mitochondria (▲) and long apical microvilli (Mv) surrounding the outer segment of the photoreceptor. POS appears as elongated, straight structures. Parallel lamellar discs of the photoreceptors outer segments can be seen (*). Choriocapillary layer can be noticed (Ch) (TEM, X2000)



Print Mag: 11700x @ 7.0 in
2 microns
HV=80.0kV
Direct Mag: 2000x

Fig. 24: A transmission electron micrograph of a section in the retina of group II (affected group) showing retinal pigmented cell (RPE). RPE is resting on Bruch's membrane (thick white arrow) with extensively destructed broken apical microvilli (Mv), oval nucleus (N) with areas of karyolysis (curved arrow) and large phagosomes (ph). The photoreceptor outer segments (POS) are disorganized and vacuolated (V). There are wide areas of lost photoreceptors outer segments (thick black arrow). (TEM, X2000)

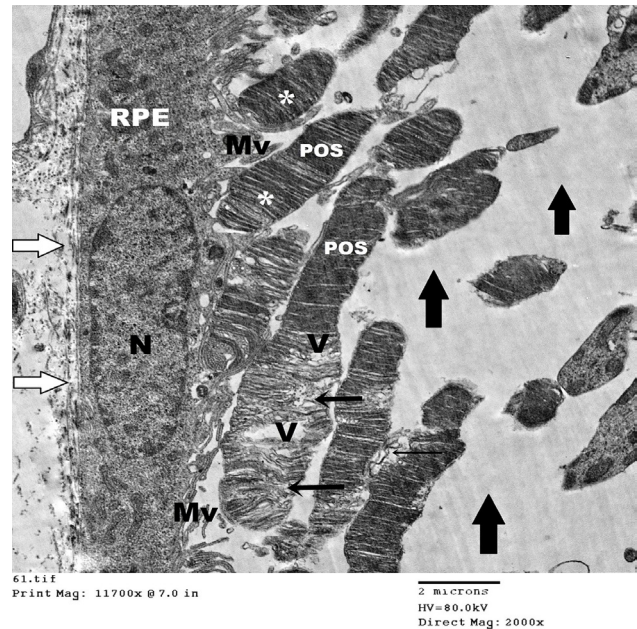


Fig. 25: A transmission electron micrograph of a section in the retina of group III (DR + SC) showing retinal pigmented cell (RPE) resting on distorted Bruch's membrane (thick white arrow). RPE has large oval nucleus (N) and broken apical microvilli (Mv). Some photoreceptors outer segments (POS) are present with normal lamellar appearance (*) and others with loss of normal orientation of their lamellar disc membranes (black †) and vacuolation (V). There are areas of loss of photoreceptors outer segments (thick black arrow) (TEM, X2000)

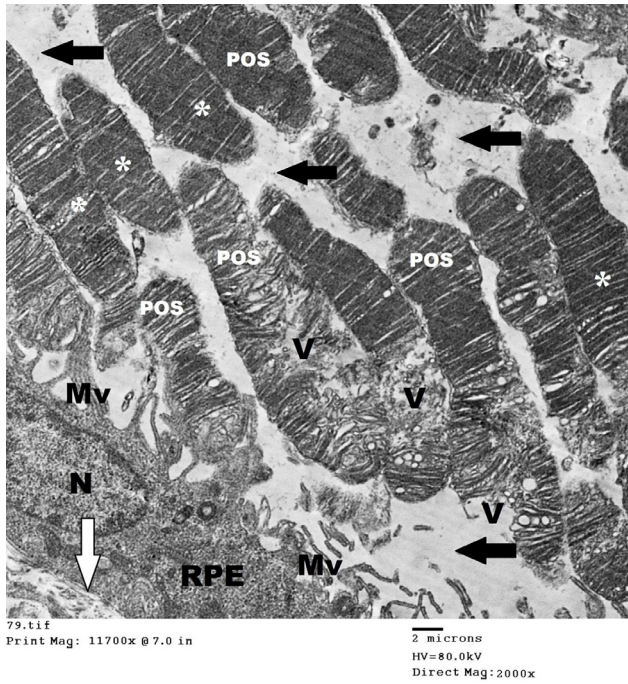


Fig. 26: A transmission electron micrograph of a section in the retina of group IV (DR + Exosomes) showing retinal pigmented cell (RPE) resting on Bruch's membrane (thick white arrow) with nearly normal oval nucleus (N) and apical microvilli (Mv). Multiple photoreceptors outer segments (POS) are present slightly separated by spaces (thick black arrow). Some of these segments have normal lamellar appearance (*), and others showing vacuolation (V). (TEM, X2000)

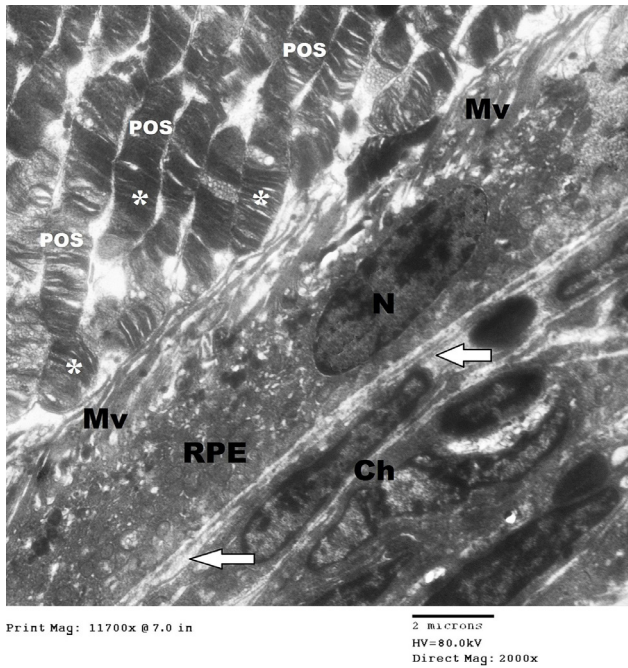


Fig. 27: A transmission electron micrograph of a section in the retina of group V (DR + SC + Exosomes) showing nearly normal Retinal pigment epithelium (RPE) resting on Bruch's membrane (Thick white arrow) separating it from the Choriocapillary layer (Ch). RPE has large oval heterochromatic nucleus (N) and many long apical microvilli (Mv) enclosing the outer segments. The photoreceptors outer segments (POS) are nearly normal with lamellar membranous discs (*). (TEM, X2000)

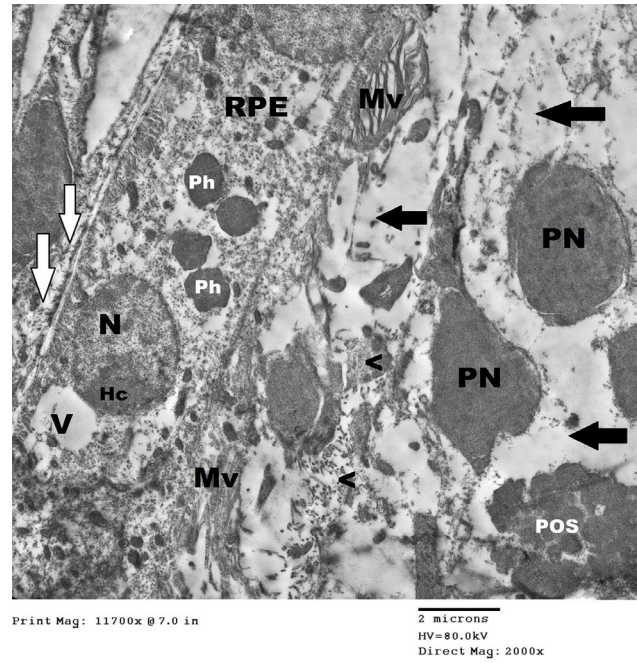


Fig. 28: A transmission electron micrograph of a section in the retina of group VI (recovery group) showing retinal pigmented cell (RPE) resting on Bruch's membrane (thick white arrow) with distorted apical microvilli (Mv), large phagosomes (ph), vacuolated cytoplasm (V) and oval nucleus (N) showing areas of heterochromatin (Hc). The photoreceptor outer segments (POS) are markedly distorted and shrunken. There are large areas of degeneration (thick black arrow) filled with debris (<). Notice the protrusion of some photoreceptors nuclei (PN) into the area of the outer segments. (TEM, X2000).

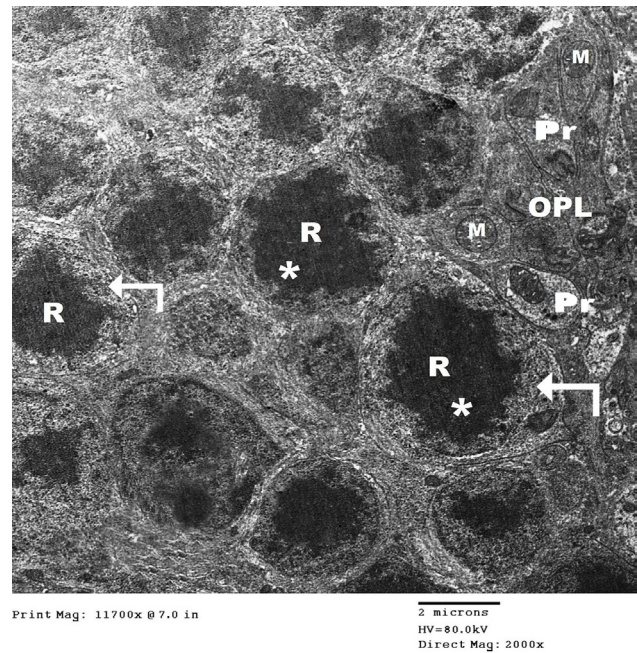
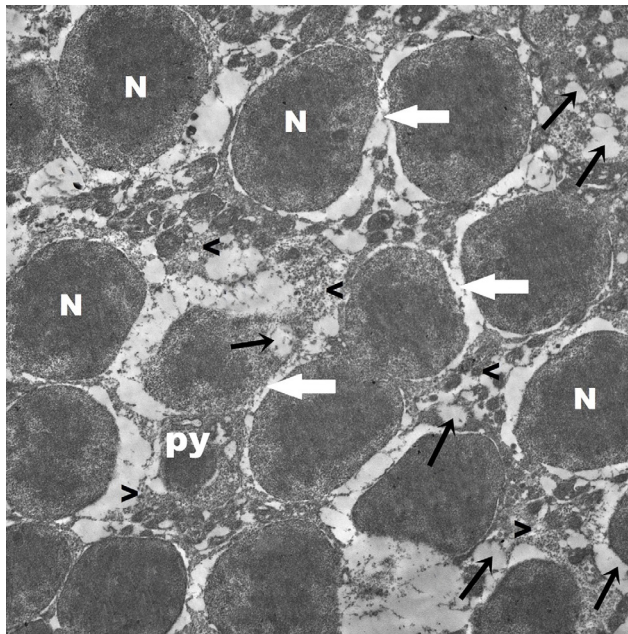
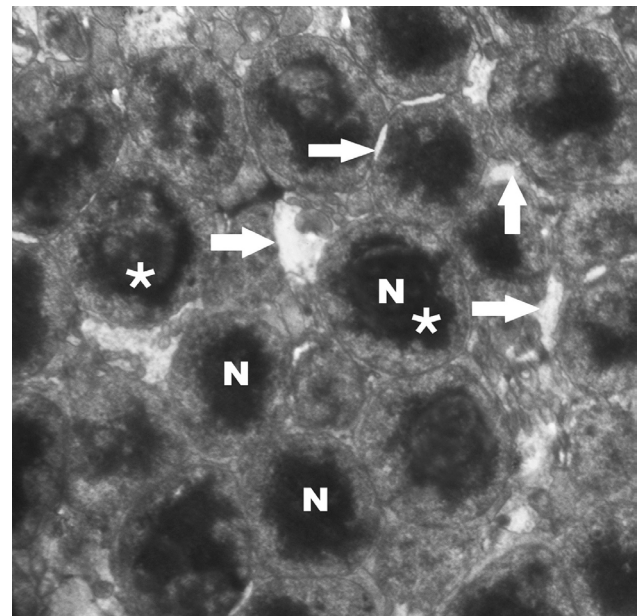


Fig. 29: A transmission electron micrograph of a section in the retina of group I (control group) showing outer nuclear layer with the predominate rod cells (R). Their nuclei are rounded with highly condensed centrally located heterochromatin (*), and surrounded by a thin rim of cytoplasm (angled arrow). Notice the cells are tightly backed with no intercellular spaces. Small area of the outer plexiform layer (OPL) can be seen, with many processes (Pr) containing Mitochondria (M). (TEM, X2000)



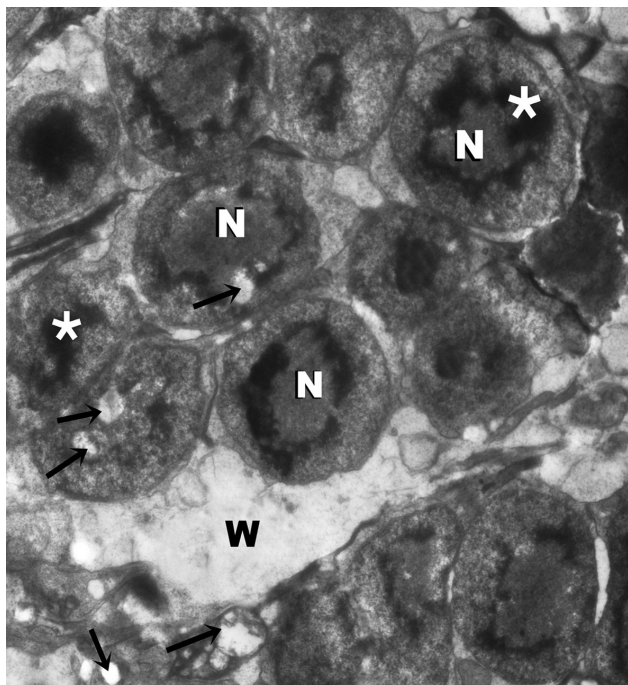
Print Mag: 11700x @ 7.0 in
 2 microns
 HV=80.0kV
 Direct Mag: 2000x

Fig. 30: A transmission electron micrograph of a section in the retina of group II (affected group) from the outer nuclear layer showing many photoreceptors nuclei (N). Cells showing severe cytoplasmic vacuolization (black ↑). The nuclei are separated by intercellular spaces (thick white arrow) filled with debris (>). pyknotic nucleus can be seen (Py). (TEM, X2000)



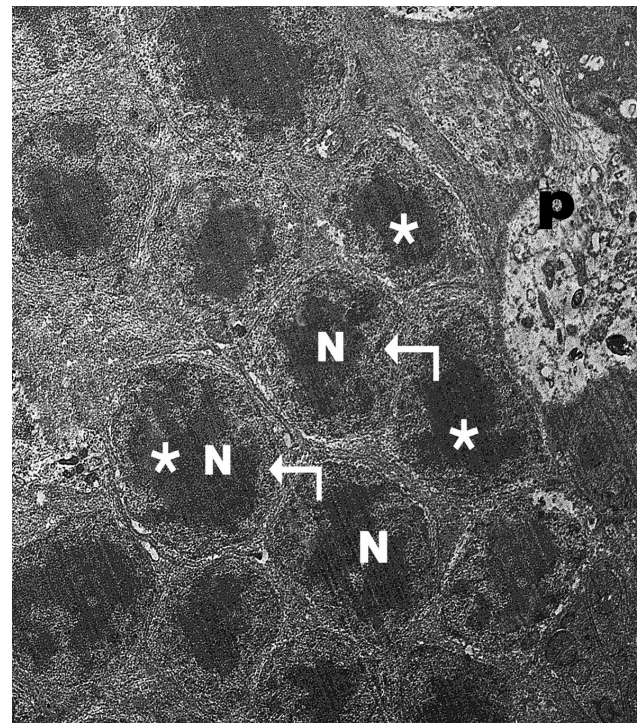
Print Mag: 11700x @ 7.0 in
 2 microns
 HV=80.0kV
 Direct Mag: 2000x

Fig. 32: A transmission electron micrograph of a section in the retina of group IV (DR + Exosomes) from the outer nuclear layer showing many nuclei (N) with heterochromatin (*). little intercellular spaces separate some cells (thick white arrow). (TEM, X2000)



Print Mag: 11700x @ 7.0 in
 2 microns
 HV=80.0kV
 Direct Mag: 2000x

Fig. 31: A transmission electron micrograph of a section in the retina of group III (DR + SC) from the outer nuclear layer showing many nuclei (N) with heterochromatin (*). Wide area separating some nuclei can be seen (W). Many cytoplasmic vacuolations (black ↑) are noticed. (TEM, X2000)



74.tif
 Print Mag: 11700x @ 7.0 in
 2 microns
 HV=80.0kV
 Direct Mag: 2000x

Fig. 33: A transmission electron micrograph of a section in the retina of group V (DR+ SC+ Exosomes) from the outer nuclear layer showing nearly normal nuclei (N) with heterochromatin (*) surrounded by thin rim of cytoplasm (angled arrow) with no intercellular spaces between cells. Process of muller cell can be noticed with electron lucent cytoplasm and different organelles (P) (TEM, X2000)

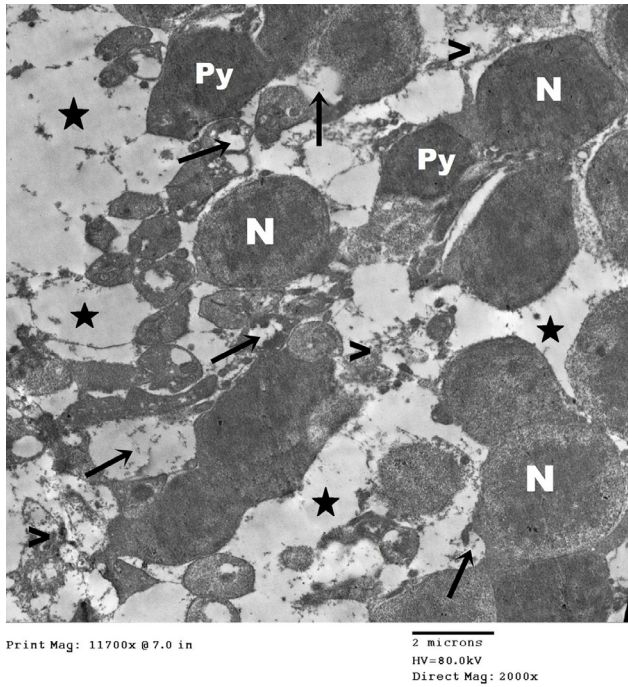


Fig. 34: A transmission electron micrograph of a section in the retina of group VI (recovery group) from the outer nuclear layer showing many nuclei (N). Degenerated cells with severe cytoplasmic vacuolization (black ↑). Some areas are showing complete dissolution of photoreceptor nuclei (star) and filled with debris (>). Some other pyknotic nuclei are present (Py). The number of photoreceptor cell nuclei has decreased. (TEM, X2000)

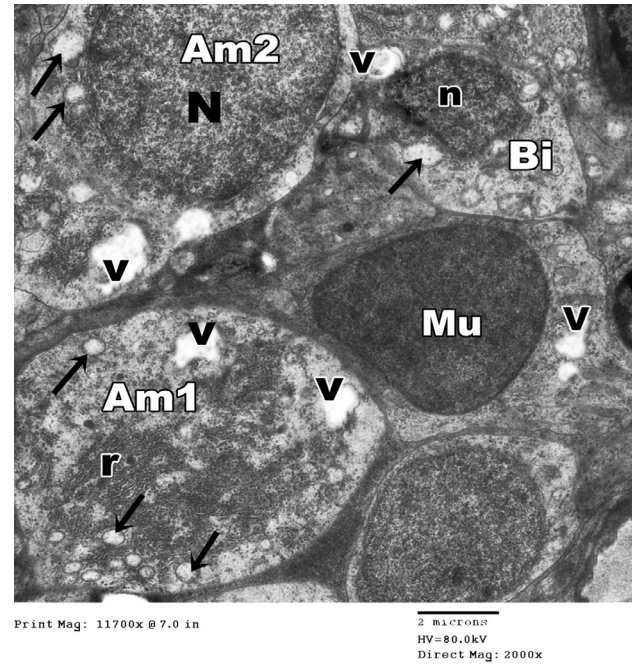


Fig. 36: A transmission electron micrograph of a section in the retina of group II (affected group) from the inner nuclear layer showing many cytoplasmic vacuolation (V) and mitochondria with destructed cristae (↑) in its cells. One amacrine cell (Am1) appears with disintegrated cytoplasm filled with rough endoplasmic reticulum (r). Another amacrine cell (Am2) showing large nucleus (N) with heterochromatin. Bipolar cell (Bi) showing shrunken nucleus (n) with peripheral heterochromatin. A Müller cell can be seen (Mu). (TEM, X2000)

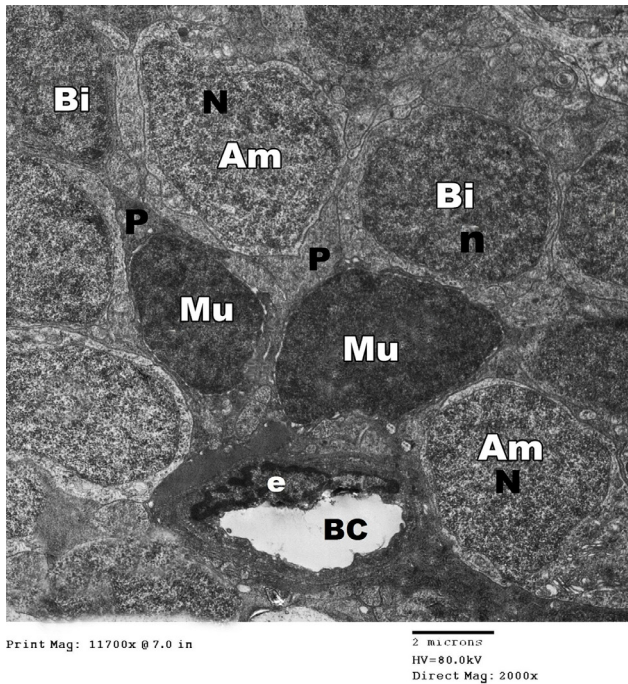


Fig. 35: A transmission electron micrograph of a section in the retina of group I (control group) from the inner nuclear layer showing amacrine cells (Am) with large and pale euchromatic nuclei (N). Müller cells (Mu) have dense nucleus and irregular outlines with prominent processes (P). The cell bodies of bipolar cells (Bi) show round nuclei (n). Normal retinal blood capillary (BC) lined with endothelial cell (e) can be observed. (TEM, X2000)

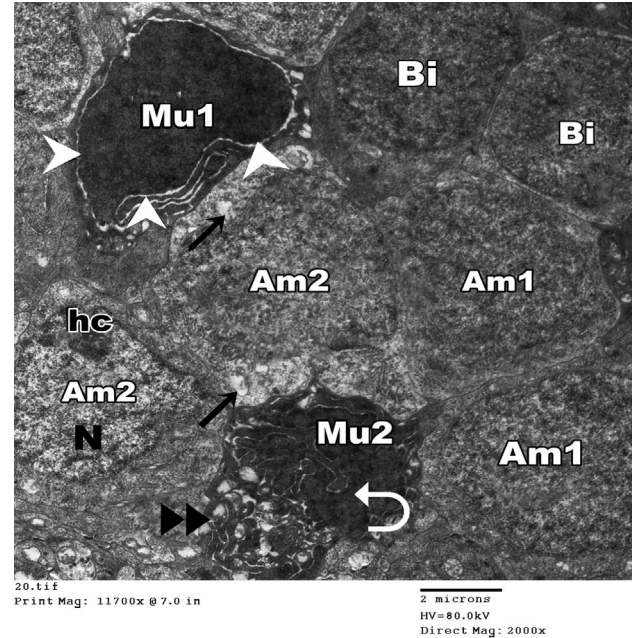


Fig. 37: A transmission electron micrograph of a section in the retina of group III (DR + SC) from the inner nuclear layer showing some normal bipolar (Bi) and amacrine cells (Am1). Another amacrine (Am2) cell showing shrunken nucleus (N) with areas of peripheral heterochromatin (hc). One Müller cell (Mu1) appears irregular in shape with dark irregular nucleus showing dilated nuclear envelope (arrow head). Another Müller cell (Mu2) showing shrunken and indented nucleus (curved arrow) and phagocytic material and electron dense bodies (▶▶). Some mitochondria with destructed cristae can be detected (↑). Bipolar cells (Bi) appear nearly normal. (TEM, X2000)

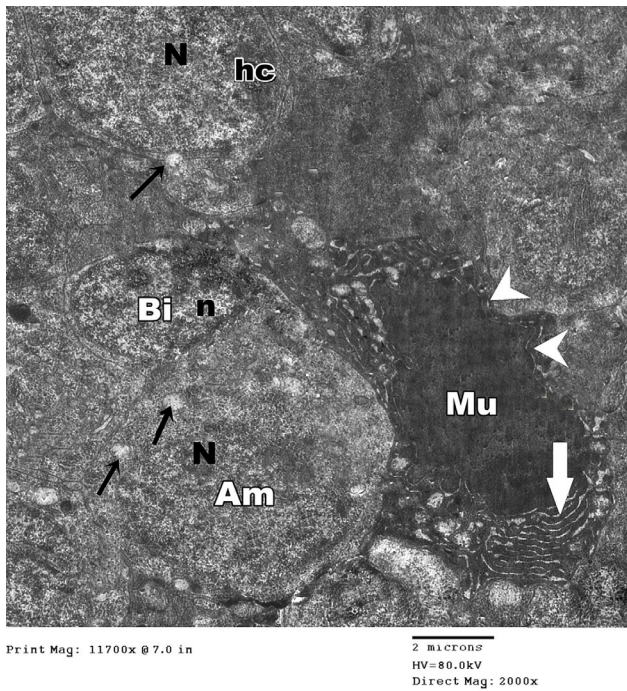


Fig. 38: A transmission electron micrograph of a section in the retina of group IV (DR + Exosomes) from the inner nuclear layer showing an amacrine cell (Am) having normal nucleus (N). The cytoplasm showing mitochondria with destructed cristae (†). Müller cell (Mu) showing large irregular dense nucleus with dilated nuclear envelope (arrow heads) and dilated RER (thick white arrow). (TEM, X2000)

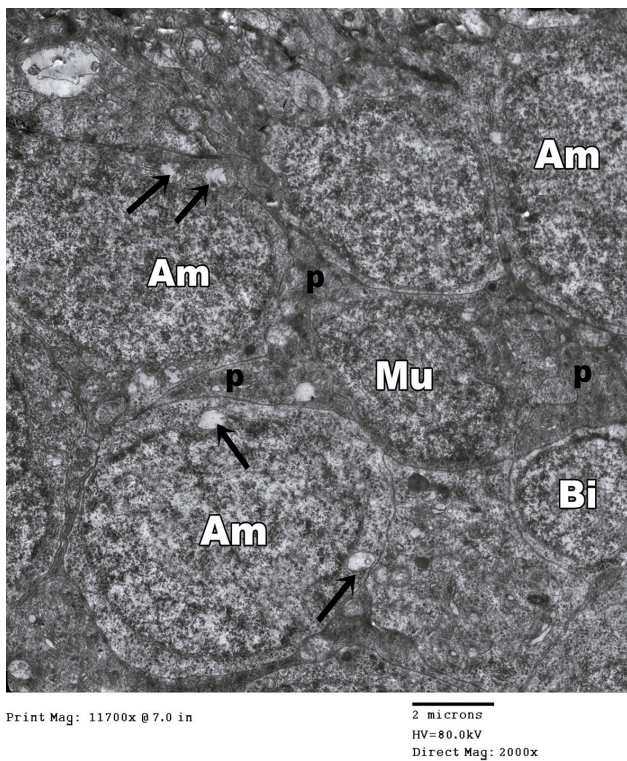


Fig. 39: A transmission electron micrograph of a section in the retina of group V (DR + SC + Exosomes) from the inner nuclear layer showing nearly normal amacrine (Am). Bipolar cells (Bi) appear with destructed mitochondrial cristae (†). Müller cell (Mu) appear with irregular outlines and prominent processes (P). (TEM, X2000)

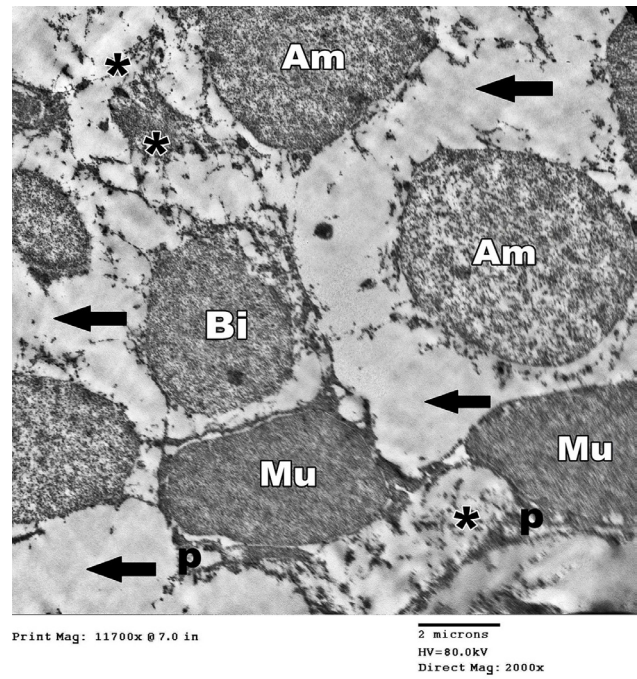


Fig. 40: A transmission electron micrograph of a section in the retina of group VI (recovery group) from the inner nuclear layer showing degenerated amacrine cells (Am) and bipolar cell (Bi) with decrease in the cell density. The cells are at various stages of disintegration and most of their cytoplasmic organelles are absent. The empty spaces left by degenerated cell bodies and processes (thick black arrow) are filled with debris (*) Müller cells (Mu) appear with irregular thin cytoplasmic processes (p). (TEM, X2000)

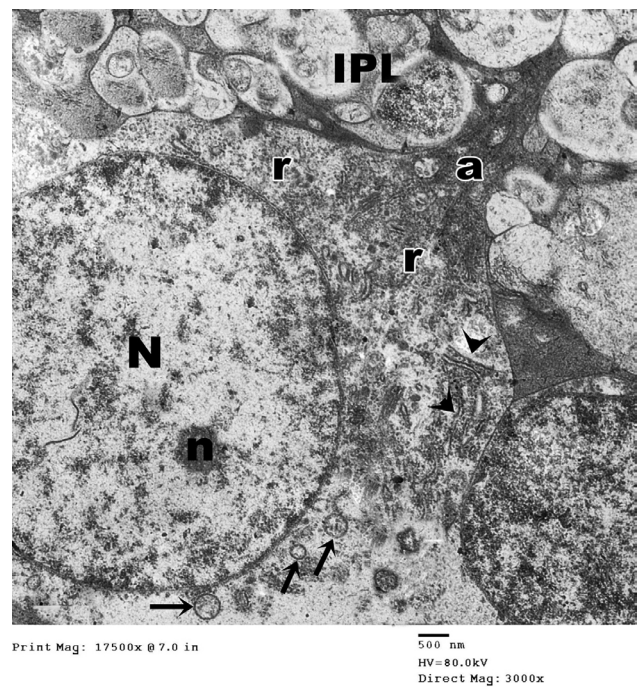


Fig. 41: A transmission electron micrograph of a section in the retina of group I (control group) from the ganglion cell layer showing ganglionic cell having large rounded euchromatic nucleus (N) with uniformly staining nucleoplasm and prominent nucleolus (n). Few mitochondria (†), Rough endoplasmic reticulum (arrow heads) and scattered ribosomes (r) are observed. Ganglion cell axon developed from a portion of the axon hillock (a). Parts of inner plexiform layer (IPL) are seen. (TEM, X3000)

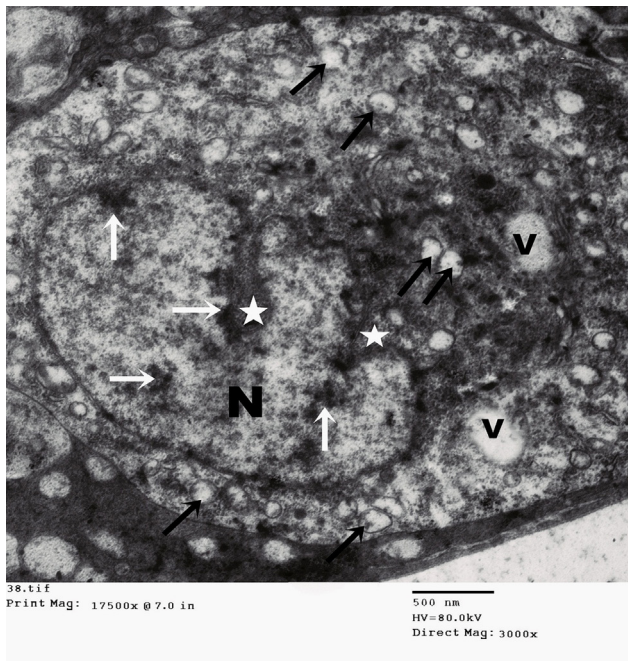


Fig. 42: A transmission electron micrograph of a section in the retina of group II (affected group) from the ganglion cell layer showing ganglion cell with indented nucleus (N) exhibiting highly convoluted sinuses (star) and areas of electron-dense heterochromatin (white ↑). Swollen mitochondria (black ↑) with disintegrated cristae and decreased matrix density can be noticed. The cytoplasm shows vacuolations (v). (TEM, X3000)

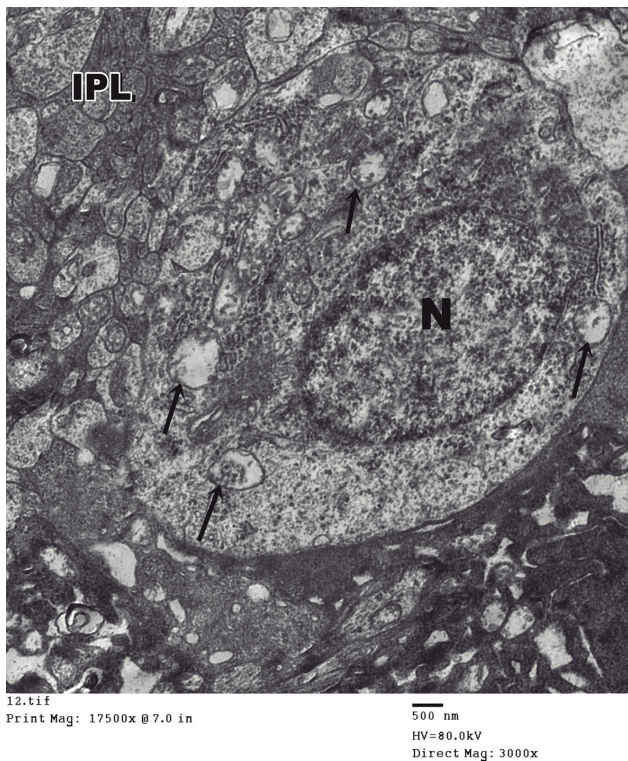


Fig. 43: A transmission electron micrograph of a section in the retina of group III (DR + SC) from ganglion cell layer showing ganglionic cell with oval granular nucleus (N). The cytoplasm showed swollen mitochondria with destructed cristae (↑). Part of the inner plexiform layer (IPL) can be seen. (TEM, X3000)

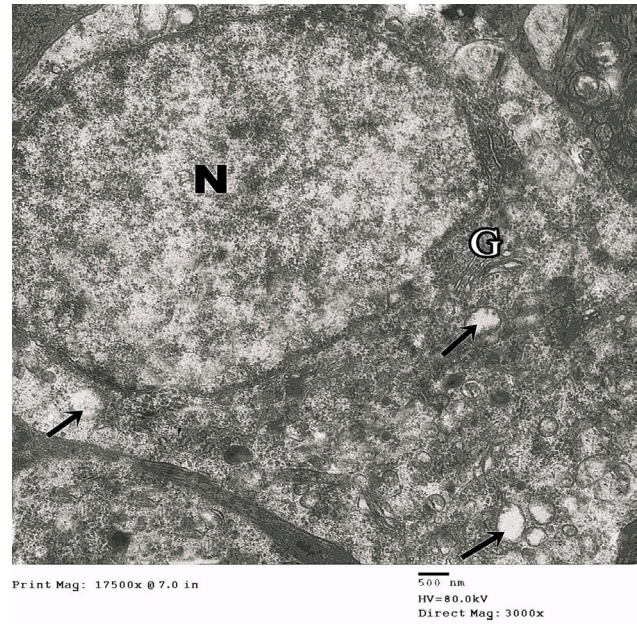


Fig. 44: A transmission electron micrograph of a section in the retina of group IV (DR + Exosomes) from ganglion cell layer showing ganglion cell with large euchromatic nucleus (N). Some mitochondria appear swollen with destructed cristae (↑). Prominent normal Golgi apparatus was seen (G). (TEM, X3000)

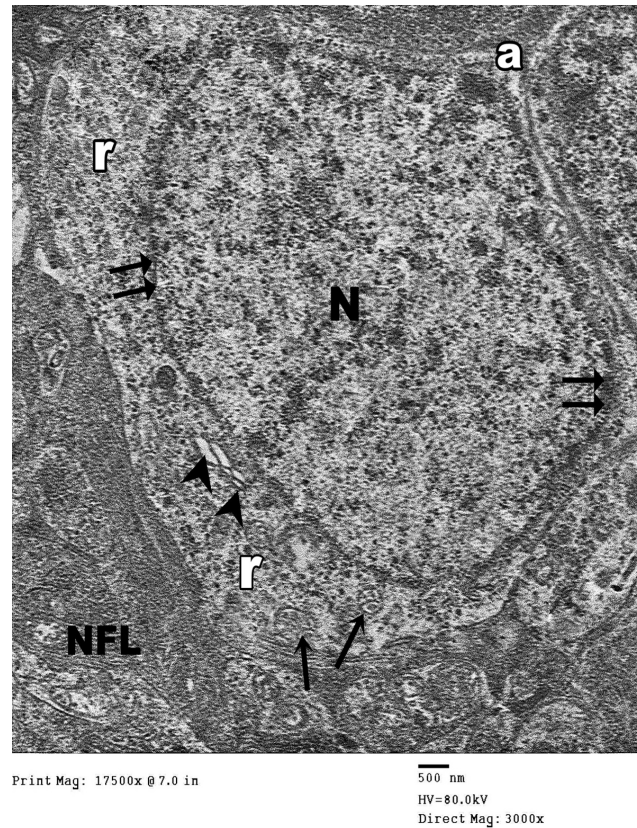


Fig. 45: A transmission electron micrograph of a section in the retina of group V (DR + SC + Exosomes) from ganglion cell layer showing nearly normal ganglion cell with large oval euchromatic nucleus (N) and normal nuclear membrane (↑↑). The cytoplasm contains plenty of ribosomes (r), slightly dilated RER (arrow head) and slightly swollen mitochondria (↑). Ganglion cell axon developed from a portion of the axon hillock (a). Part of the nerve fiber layer (NFL) is observed. (TEM, X3000)

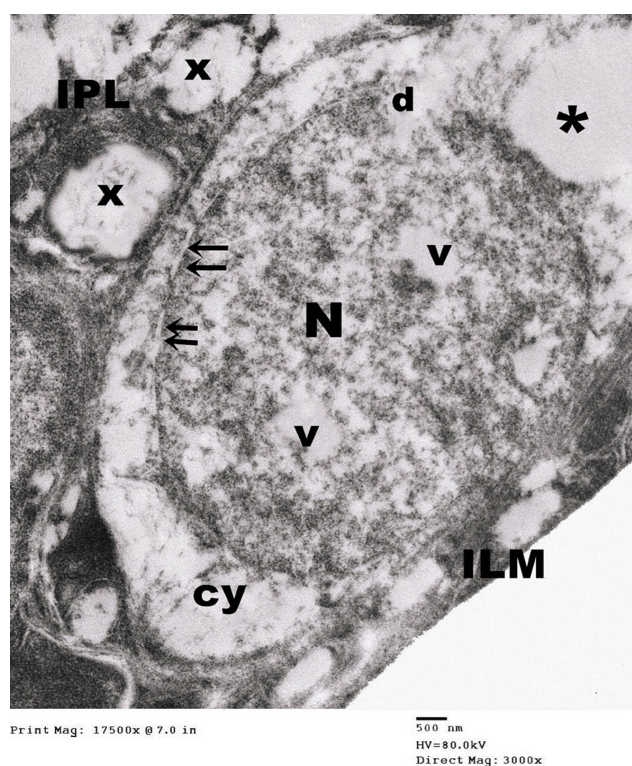


Fig. 46: A transmission electron micrograph of a section in the retina of group VI (recovery group) from the ganglion cell layer of the retina showing ganglion cell with highly rarefied cytoplasm (cy) containing large vacuoles (*). Nucleus is granular (N) and showing karyolysis (k), slightly dilated nuclear envelope (↑↑). Area of disrupted envelope (d) can be noticed. The inner limiting membrane (ILM) appears abnormal and the inner plexiform layer (IPL) shows destructed axons (x). (TEM, X3000)

Table 1: Showing the mean area % and ±SD of VEGF expression of all groups

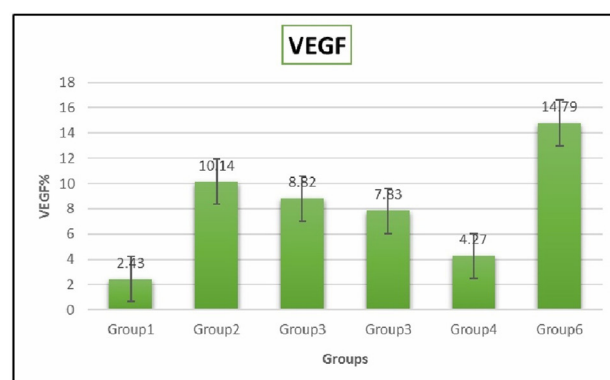
	Group I	Group II	Group III	Group IV	Group V	Group VI
VEGF Mean (%)	2.43	10.14	8.82	7.83	4.27	14.79
±SD	0.41	1.69	1.47	1.31	0.71	2.47
Significant at $P < 0.05$	b,c,d,e,f	a,c,d,e,f	a,b,d,e,f	a,b,c,e,f	a,b,c,d,f	a,b,c,d,e

Data expressed as mean ±SD SD: standard deviation
 Test used: One-way ANOVA followed by post-hoc tukey
 a: significance relative to Group I b: significance relative to Group II
 c: significance relative to Group III d: significance relative to Group IV
 e: significance relative to Group V f: significance relative to Group VI

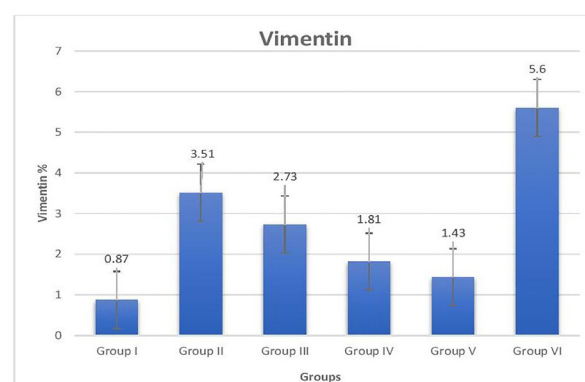
Table 2: Showing the mean area % and ± SD of Vimentin expression of all groups

	Group I	Group II	Group III	Group IV	Group V	Group VI
vimentin Mean (%)	0.87	3.51	2.73	1.81	1.43	5.6
±SD	0.14	0.59	0.46	0.30	0.24	0.93
Significant at $P < 0.05$	b,c,d,e,f	a,c,d,e,f	a,b,d,e,f	a,b,c,e,f	a,b,c,d,f	a,b,c,d,e

Data expressed as mean ±SD SD: standard deviation
 Test used: One-way ANOVA followed by post-hoc tukey
 a: significance relative to Group I b: significance relative to Group II
 c: significance relative to Group III d: significance relative to Group IV
 e: significance relative to Group V f: significance relative to Group VI



Histogram 1: showing the mean area % of VEGF expression in all groups



Histogram 2: showing the mean area % of vimentin expression in all groups

DISCUSSION

Diabetic retinopathy is one of the most substantial microvascular complications of diabetes mellitus and is the commonest cause of blindness in people under the age of 6 [23]. All persons with diabetes are at risk of developing retinopathy, however, persons with type 1 diabetes (T1DM) have a higher chance [24].

Streptozotocin (STZ) was used in this study as it considered the most widely accepted animal model for the evaluation of retinal complications in diabetes and this agreed with a previous study [25] which reported that STZ induces various biochemical and histological alterations closely resemble the initial process of diabetic retinopathy that occurs in humans.

The mechanism of diabetes mellitus induction by STZ was explained in former study [26] that STZ is a toxic glucose analogue that accumulates in pancreatic β-cells via uptake by the GLUT2 glucose transporter. STZ is split into its glucose and methyl nitrosurea moiety. The latter is a powerful alkylating agent that induces multiple DNA strand breaks and fragmentation causing β-cell damage.

Group II of the present study showed decreased retinal thickness, signs of degenerated cells (RPE, ONL, INL and GCL), dilated congested new blood vessels. These results agreed with some investigators [27-28] and were explained by Roy *et al.* [29] who clarified that in diabetic retinopathy, mitochondrial dysfunction, endoplasmic reticulum stress,

and subsequent breakdown of cellular homeostasis play a critical role in retinal cell death. Retinal mitochondrial dysfunction begins early in diabetes and is known to contribute to DR pathology. Mitochondrial dysfunction increases production of neurotoxic ROS and is also expected to result in primary energetic deficits that are detrimental to retinal neurons^[30].

Our study showed marked significant increase ($P < 0.05$) in VEGF and Vimentin immunostaining, which agreed with previous studies^[31-32]. Overexpression of vimentin occurs during Müller cell gliosis, which is known to be increased in STZ induced diabetic retinopathy. Increased retinal gliosis in the diabetic group was clarified by previous author^[12] who stated that, in the early stages of STZ induced diabetes, the neuronal and glial alterations in the retina precede the typical vascular changes. Normally after about 6 weeks of induction of diabetes, Müller cell gliosis and neuronal deficits begin to become prominent.

Diabetic retinopathy is associated with neovascularization which caused by an imbalance of pro-angiogenic mediators and ischemia resulting in abnormal growth of new vessels, which hinders with the normal function of the retina, specifically light transmission. The consequences are leaky vessels and an accumulation of fluids and proteins. The major regulator pro-angiogenic factor is VEGF, which increased after hyperglycemia and hypoxia. An imbalance in the expression of VEGF is responsible for the increased neovascularization in DR^[2]. Intraocular VEGF expression is markedly upregulated in diabetes. VEGF damages BRB not only through breaking endothelial tight junctions, increasing vascular permeability, and leading to retinal edema but also through inducing leukocyte aggregation, touching off inflammatory response, and injuring endothelial cells. The inflammation in sequence stimulates further release of VEGF^[33].

Most of the established therapies target quite advanced states of DR. It is desirable to develop strategies targeting early phases in DR to delay or even prevent this critical complication^[34]. Stem cell therapy has become one of the most promising therapeutic strategies for DR with the development of modern medical technology in the field of gene and stem cell therapy^[35].

The Stem cell group (group III) in the present study showed slightly increased retinal thickness with some small congested blood vessels. There was little decrease in VEGF and Vimentin immunostaining compared to group II.

These results were compatible and confirming the findings of previous investigator^[12] who reported that injection of bone marrow derived-MSCs demonstrated selective protection against retinal gliosis and increased vascular integrity in an induced diabetic retinopathy rat model. Also, another research^[36] focused on the ROS-induced damage to the neurovascular unit of the retina, to find that retinal ganglion cells death, vascular leakage, apoptosis and inflammation were obviously downregulated when MSC were injected.

Some researchers^[37-38] explained that, MSCs exert at least a dual role in DR. First, these seem to resume a pericyte function, acquiring perivascular localization and endothelial cell enwrapping. By this, MSCs appears to adopt pericyte regulatory functions, monitoring survival and proliferation. Second, they secrete a variety of trophic factors which control the local adverse environment by regulating oxidative stress, inflammation and integrity of the neurovascular unit. Also, another study^[39] reported that neuroprotective growth factors such as brain-derived neurotrophic factor (BDNF), ciliary-derived neurotrophic factor (CNTF), nerve growth factor (NGF), glial-derived neurotrophic factor (GDNF), and basic fibroblast growth factor (bFGF) were meaningfully increased in DR rats injected with MSCs.

The significant decrease in VEGF immunoreactivity ($P < 0.05$) explained by another study^[36] stated that MSCs exerted cytoprotective action through secretion of platelet-derived anti-angiogenic factor, Thrombospondin Type-1 (TSP-1), which is also produced primarily from the RPE, choroid, and Müller glial cells. TSP-1 is a glycoprotein that controls MSC functions including anti-angiogenic, anti-inflammatory, as well as immunomodulatory and immune-privileged activities.

In contrast, some investigators^[40-42] noticed that after the transplantation of MSCs into the vitreous, the cells could not be maintained for a long time. They showed that hyperglycemia caused BM-MSC abnormality via overproduction of advanced glycation end product (AGE), which induced low proliferation, senescence, apoptosis and abnormal differentiation in vitro. Also, some investigators^[12] demonstrated an increased expression of Vimentin after intravitreally transplanted BMSCs which indicates that these cells may have been differentiated to Muller glia, as Vimentin is marker of Muller cells.

Regardless the benefits of MSCs, some researchers^[43,44] addressed the potential risks associated with cell injection. They addressed retinal glial responses (graft-induced reactive gliosis) upon intravitreally injected rat BM-MSC.

Exosomes are an attractive target for clinical research, as they can offer comparable therapeutic effects of mesenchymal stem cells without the potential adverse effects associated with cell therapy^[45]. The advantages of using exosomes instead of live cells are connected to their minimal immunogenicity, low inherent toxicity, and potentially lower risk for tumor formation. Moreover, because of their chemical composition and small size, EXOs may easily diffuse across the biological barriers reaching target cells^[46].

Group IV of this study revealed moderate improvement in the retinal histology with little spaced nuclei in ONL and INL and vacuolated ganglion cell. There was a significant decrease ($P < 0.05$) in VEGF and Vimentin immunostaining compared to group II,

These outcomes are in concurrence with those of^[47] who showed that mesenchymal stem cells-derived

exosomes ameliorate blue light stimulation in retinal pigment epithelium cells and retinal laser injury and concluded that, MSC-Exosomes might be optimal candidates for intravitreal injection, which could actually overcome the obstacles and risks related to stem cell transplantation therapy, such as possible long-term pathological differentiation, vitreous opacities, and poor preservation. Also, a previous study^[48] findings showed that intravitreal injection of exosomes from human MSCs was well-tolerated and significantly decreased the degree of retinal ischemia and neovascularization in Oxygen-induced retinopathy (OIR) model.

Interestingly, MSC exosomes also contain antiangiogenic miRNAs such as miR-16 and miR-100 that suppress angiogenesis by targeting vascular endothelial growth factor (VEGF) in breast cancer cells within a tumor microenvironment^[49]. Consecutively, another study^[50] showed that MSCs-Exos could inhibit the neovascularization by inhibiting NF- β signaling β and by downregulation of VEGF expression that might be influenced by vital proteins or RNAs encapsulated in MSC-Exosomes.

Some authors^[7] compared the effect of intravitreal injection of MSC-Exos and MSCs using an animal model of laser-induced retinal injury and found that the protective effect of MSC-Exosomes on injured retina was equal to that of MSCs in limiting the damage extent, reducing apoptosis, and inhibiting inflammatory responses.

On the other hand, some müller cells appeared with dilated rough endoplasmic reticulum (rER) indicating secretory activity. This was explained by some researchers^[51] who clarified that when the retina is damaged, injected MSCs can differentiate into Müller cells, which in turn can dedifferentiate and proliferate, generated neuronal progenitor cells, migrate to the injured retinal regions, and differentiate into lost neuronal types.

The MSCs and exosomes group (group V) in the present study showed nearly normal retinal histology and the same ultrastructure of the retina except little vacuolation in GC, and INL cells. There was significant decrease ($P < 0.05$) in VEGF and Vimentin immunostaining compared to group II, III & IV.

Parallel to our results, a recent rat study^[52] demonstrated that combined MSCs and MSC-Exosomes delivery was better in terms of brain protection and neurological recovery when compared with MSC transplantation or EV injection only. A previous researcher^[53] indicated that co-administration of MSCs and their conditioned media could regulate the hyperglycemia in diabetic rats more than either group alone. Therefore, it could be assumed that there is synergistic effect between MSCs and supernatant of MSCs in pancreatic regeneration of diabetic animals.

Also, another investigator^[54] explained that MSC-derived exosomes have a key role in mediating the ability of MSCs to function as stromal support cells to maintain

homeostasis within the tissue and respond to external stimuli.

Retinal Samples of group VI that were taken 12 weeks after induction of diabetes showed no improvement in the histological and immunostaining results but worsen signs of degenerated retinas representing irreversibility of STZ induced diabetic retinopathy. Our results agreed with previous studies^[55-57] displayed that the pathomorphological changes of INL and ONL, thinning of the retinal layers, the number of new blood vessels and mRNA expression of VEGF were all increased in retinas of diabetic rats at both 3, 4 months after the development of diabetes, compared to 2 months after diabetes. This was explained by previous research^[28] who stated that STZ-induced type 1 diabetic rat model does not experience self-remission or recovery over time as a result of the STZ-induced permanent destruction of islet β cells.

CONCLUSION

This work concluded that BMSCs and their exosomes can treat diabetic retinopathy, but their combination gives better results.

CONFLICTS OF INTEREST

There are no conflicts on interest

REFERENCES

1. Reddy YK, Chitra S, Reddy BS, Jeykodi S, Deshpande JM, and Juturu V. Soluble Lutein Protects Eye Lens for Cataract Development and Progression in Streptozotocin-Induced (STZ) Diabetic Rats. *EC Ophthalmology* 2018; 9(2): 76-84.
2. Altmann C, Schmidt MHH. The Role of Microglia in Diabetic Retinopathy: Inflammation, Microvasculature Defects and Neurodegeneration. *Int J Mol Sci.* 2018;19(1): 1-13.
3. Gu X, Yu X, Zhao C, Duan P, Zhao T, Liu Y, Li S, Yang Z, Li Y, Qian C, Yin Z. and Wang Y. Efficacy and Safety of Autologous Bone Marrow Mesenchymal Stem Cell Transplantation in Patients with Diabetic Retinopathy. *Cell Physiol Biochem.* 2018;49(1):40-52
4. Kramerov AA, Ljubimov AV. Stem cell therapies in the treatment of diabetic retinopathy and keratopathy. *Exp Biol Med (Maywood).* 2015; 241 (6): 559–568.
5. Yolanda MM, Maria AV, Amaia FG, Marcos PB, Silvia PL, Dolores E. and Jesús O. Adult stem cell therapy in chronic wound healing. *J. Stem Cell Res. Ther.* 2014; 4 (1): 1-6.
6. Gater R, Nguyen D, Haj AJE, Yang Y. Development of Better Treatments for Retinal Disease Using Stem Cell Therapies. *Int J Stem Cell Res Ther.* 2016; 3: 1-6.

7. Yu B, Shao H, Su C, Jiang Y, Chen X, Bai L, Zhang Y, Li Q, Zhang X, & Li X. Exosomes derived from MSCs ameliorate retinal laser injury partially by inhibition of MCP-1. *Sci Rep.* 2016;(6): 1-12.
8. Yin K, Wang S. and Zhao RC. Exosomes from mesenchymal stem /stromal cells: a new therapeutic paradigm. *Biomark Res.* 2019; 7:1-8.
9. Rashed M, Bayraktar E, K Helal G, Abd-Ellah MF, Amero P, Chavez-Reyes A, Rodriguez-Aguayo C. Exosomes: From Garbage Bins to Promising Therapeutic Targets. *Int J Mol Sci.* 2017; 18(3): 1-25.
10. Beer L, Mildner M, Ankersmit HJ. Cell secretome based drug substances in regenerative medicine: when regulatory affairs meet basic science. *Ann Transl Med.* 2017;5 (7):1-3.
11. Ebrahim N, Ahmed IA, Hussien NI, Dessouky AA, *et al.* Mesenchymal Stem Cell-Derived Exosomes Ameliorated Diabetic Nephropathy by Autophagy Induction through the mTOR Signaling Pathway. *Cells* 2018; 7(12):1-26.
12. Çerman E, Akkoç T, Eraslan M, *et al.* Retinal Electrophysiological Effects of Intravitreal Bone Marrow Derived Mesenchymal Stem Cells in Streptozotocin Induced Diabetic Rats [published correction appears in *PLoS One* 2016;11(6):1-11.
13. Baghaei K, Hashemi SM, Tokhanbigli S, Asadi A, *et al.* Isolation, differentiation, and characterization of mesenchymal stem cells from human bone marrow. *Gastroenterol. Hepatol. Bed. Bench.* 2017;10 (3): 208-213.
14. El Said, H.E.; Gabr, H.M. and Ammar, R.I. The effect of human bone marrow mesenchymal stem cells on diabetic heart failure rats. *Life Sci. J.* 2013; 10 (1): 3413-3425
15. Bruno S, Grange C, Collino F, Deregibus MC, *et al.* Microvesicles Derived from Mesenchymal Stem Cells Enhance Survival in a Lethal Model of Acute Kidney Injury. *PLoS ONE* 2012;7(3):1-11.
16. Safwat A, Sabry D, Ragiae A, Amer E, *et al.* Adipose mesenchymal stem cells-derived exosomes attenuate retina degeneration of streptozotocin-induced diabetes in rabbits. *J Circ Biomark* 2018;7: 1-10.
17. Bancroft JD and Layton C. The hematoxylin and eosin, In: Suvarna SK, Layton C and Bancroft JD, editors. *Bancroft's Theory and practice of histological* 7th edition. Churchill Livingstone: Philadelphia. 2013:173-212.
18. Van der Loos CM, Meijer-Jorna LB, Broekmans ME, *et al.* Anti-human vascular endothelial growth factor (VEGF) antibody selection for immunohistochemical staining of proliferating blood vessels. *J Histochem Cytochem.* 2010;58(2):109–118.
19. Satelli A. and Li S. (2011): Vimentin in cancer and its potential as a molecular target for cancer therapy. *Cell. Mol. Life Sci.*; 68(18): 3033–3046.
20. Castrechini, N, Murthi, P, Gude, N.M, Erwich, J.J, Gronthos, S, Zannettino, A, Brennecke, S.P, & Kalionis, B. (). Mesenchymal stem cells in human placental chorionic villi reside in a vascular Niche. *Placenta* 2010; 31(3): 203-212.
21. Salem M, Helal O, Metwaly H. Histological and immunohistochemical study of the role of stem cells, conditioned medium and microvesicles in treatment of experimentally induced acute kidney injury in rats. *Med J Cairo Univ.* 2017; 1: 70-83.
22. Ayub B, Wani H, Shoukat S, Para PA, Ganguly S. and Ali M.: Specimen preparation for electron microscopy: an overview. *J. Environ. Life Sci.* 2017; 2 (3): 85-88.
23. Tawfik A, Mohamed R, Elsherbiny NM, DeAngelis MM, *et al.* Homocysteine: A Potential Biomarker for Diabetic Retinopathy *J. Clin. Med.*; 2019; 8 (1): 1-11.
24. Kashim RM, Newton P, Ojo O. Diabetic Retinopathy Screening: A Systematic Review on Patients' Non-Attendance. *Int J Environ Res Public Health.* 2018;15(1):1-12.
25. Jiang T, Chang Q, Cai J, Fan J, Zhang X, Xu G. Protective Effects of Melatonin on Retinal Inflammation and Oxidative Stress in Experimental Diabetic Retinopathy. *Oxid Med Cell Longev.* 2016;10: 1-13.
26. Luippold G, Bedenik J, Voigt A, Grempler R. Short- and Longterm Glycemic Control of Streptozotocin-Induced Diabetic Rats Using Different Insulin Preparations. *PLoS One.* 2016;11(6): 1-12.
27. Saxena Y, Purwar B, Meena H, Sarthi P. *Dolichos biflorus* Linn. ameliorates diabetic complications in streptozotocin induced diabetic rats. *Ayu.* 2014;35(4):442–446.
28. Yang QH, Zhang Y, Jiang J, *et al.* Protective effects of a novel drug RC28-E blocking both VEGF and FGF2 on early diabetic rat retina. *Int J Ophthalmol.* 2018;11(6):935–944.
29. Roy S, Trudeau K, Roy S, Tien T, Barrette KF. Mitochondrial dysfunction and endoplasmic reticulum stress in diabetic retinopathy: mechanistic insights into high glucose-induced retinal cell death. *Curr Clin Pharmacol.* 2013; 8(4): 278-284.

30. Pearsall EA, Cheng R, Matsuzaki S, Zhou K, Ding L, *et al.* Neuroprotective effects of PPAR α in retinopathy of type 1 diabetes. *PLoS One.* 2019; 14 (2): 1-17.
31. Fan Y, Liu K, Wang Q, Ruan Y, Zhang Y. and Ye W. Exendin-4 protects retinal cells from early diabetes in Goto-Kakizaki rats by increasing the Bcl-2/Bax and Bcl-xL/Bax ratios and reducing reactive gliosis. *Mol. Vis.* 2014; 20: 1557–1568.
32. Roy S, Trudeau K, Roy S, Tien T. and Barrette KF. Mitochondrial dysfunction and endoplasmic reticulum stress in diabetic retinopathy: mechanistic insights into high glucose-induced retinal cell death. *Curr. Clin. Pharmacol.* 2013; 8 (4): 278-284.
33. Chen W, Yao X, Zhou C, Zhang Z, Gui G, Lin B. Danhong Huayu Koufuye Prevents Diabetic Retinopathy in Streptozotocin-Induced Diabetic Rats via Antioxidation and Anti-Inflammation. *Mediators Inflamm.* 2017; (98): 1-8.
34. Park SS. Cell therapy applications for retinal vascular diseases: diabetic retinopathy and retinal vein occlusion. *Invest. Ophthalmol. Vis. Sci.* 2016 1;57(5): ORSFj1-ORSFj10
35. Paterniti I, Di Paola R, Campolo M, Siracusa R, *et al.* Palmitoylethanolamide treatment reduces retinal inflammation in streptozotocin-induced diabetic rats. *Eur J Pharmacol.* 2015; 769:313-323.
36. Ezquer M, Urzua CA, Montecino S, Leal K, Conget P, Ezquer F. Intravitreal administration of multipotent mesenchymal stromal cells triggers a cytoprotective microenvironment in the retina of diabetic mice. *Stem Cell Res Ther.* 2016; 7: 1-17.
37. Galderisi U, Giodano A. The gap between the physiological and therapeutic roles of mesenchymal stem cells. *Med Res Rev.* 2014; 34(5): 1100-1126.
38. Fiori A, Terlizzi V, Kremer H, Gebauer J, *et al.* Mesenchymal stromal/stem cells as potential therapy in diabetic retinopathy. *Immunobiology* 2018; 223 (12): 729-743.
39. Peng BY, Dubey NK, Mishra VK, Tsai FC, *et al.* Addressing Stem Cell Therapeutic Approaches in Pathobiology of Diabetes and Its Complications. *J. Diabetes Res.* 2018; (3):1-16.
40. Gravina GL, Mancini A, Colapietro A, Vitale F, *et al.* The novel CXCR4 antagonist, PRX177561, reduces tumor cell proliferation and accelerates cancer stem cell differentiation in glioblastoma preclinical models. *Tumour Biol.* 2017; 39 (6): 1-17.
41. Gu Z, Jiang J, Xia Y, Yue X, *et al.* P21 is associated with the proliferation and apoptosis of bone marrow-derived mesenchymal stem cells from non-obese diabetic mice. *Exp Clin Endocrinol Diabetes* 2013;121 (10): 607-613.
42. Khan M, Akhtar S, Mohsin S, N Khan S, Riazuddin S. Growth factor preconditioning increases the function of diabetes-impaired mesenchymal stem cells. *Stem Cells Dev.* 2011.; 20 (1):67-75.
43. Tassoni A, Gutteridge A, Barber AC, Osborne A, Martin KR Molecular mechanisms mediating retinal reactive gliosis following bone marrow mesenchymal stem cell transplantation. *Stem Cells* 2015; 33(10): 3006–3016.
44. Jian Q, Li Y, Yin ZQ. Rat BMSCs initiate retinal endogenous repair through NGF/TrkA signaling. *Exp. Exp Eye Res.* 2015;132: 34-47
45. Anderson JD, Johansson HJ, Graham CS, Vesterlund M, *et al.* Comprehensive Proteomic Analysis of Mesenchymal Stem Cell Exosomes Reveals Modulation of Angiogenesis via Nuclear Factor-KappaB Signaling. *Stem Cells* 2016;34(3):601–613.
46. Zazzeroni L, Lanzoni G, Pasquinelli G, Ricordi C. Considerations on the harvesting site and donor derivation for mesenchymal stem cells-based strategies for diabetes. *CellR4 Repair Replace Regen Reprogram.* 2017;5(5): 1-21.
47. He GH, Zhang W, Ma YX, *et al.* Mesenchymal stem cells-derived exosomes ameliorate blue light stimulation in retinal pigment epithelium cells and retinal laser injury by VEGF-dependent mechanism. *Int J Ophthalmol.* 2018;11(4): 559–566.
48. Moisseiev E, Anderson JD, Oltjen S, Goswami M, *et al.* Protective Effect of Intravitreal Administration of Exosomes Derived from Mesenchymal Stem Cells on Retinal Ischemia. *Curr Eye Res.* 2017; 42(10):1358-1367
49. Pakravan K, Babashah S, Sadeghizadeh M, Mowla SJ, *et al.* MicroRNA-100 shuttled by mesenchymal stem cell-derived exosomes suppresses in vitro angiogenesis through modulating the mTOR/HIF-1 α /VEGF signaling axis in breast cancer cells. *Cell Oncol (Dordr).* 2017; 40(5):457-470
50. Atienzar-Aroca S, Flores-Bellver M, Serrano-Heras G, Martinez-Gil N, *et al.* Oxidative stress in retinal pigment epithelium cells increases exosome secretion and promotes angiogenesis in endothelial cells. *J Cell Mol Med.* 2016; 20 (8): 1457-1466.
51. Liu Y, Wang C and Su G. Cellular Signaling in Müller Glia: Progenitor Cells for Regenerative and Neuroprotective Response in pharmacological Models of Retinal Degeneration. *J Ophthalmol.* 2019 (3): 1-14.
52. Chen KH, Chen CH, Wallace CG, Yuen CM, Kao GS, *et al.* Intravenous administration of xenogenic adipose-derived mesenchymal stem cells (ADMSC) and ADMSC-derived exosomes markedly reduced brain infarct volume and

- preserved neurological function in rat after acute ischemic stroke. *Oncotarget* 2016;7(46): 74537-74556.
53. Aali E, Mirzamohammadi S, Ghaznavi H, Madjd Z, *et al.* A comparative study of mesenchymal stem cell transplantation with its paracrine effect on control of hyperglycemia in type 1 diabetic rats. *J Diabetes Metab Disord.* 2014;13(1): 1-10.
54. Lou G, Chen Z, Zheng M. and Liu Y. Mesenchymal stem cell-derived exosomes as a new therapeutic strategy for liver diseases. *Exp Mol Med.* 2017; 49(6):1-9.
55. Li X, Zhang M, Zhou H. The morphological features and mitochondrial oxidative stress mechanism of the retinal neurons apoptosis in early diabetic rats. *J Diabetes Res.* 2014; 2014:1-8.
56. Martin PM, Roon P, Van Ells TK, Ganapathy V, Smith SB. Death of retinal neurons in streptozotocin-induced diabetic mice. *Invest Ophthalmol Vis Sci.* 2004 ;45(9):3330-3336.
57. Gong CY, Lu B, Hu QW, Ji LL. Streptozotocin induced diabetic retinopathy in rat and the expression of vascular endothelial growth factor and its receptor. *Int J Ophthalmol.* 2013; 6 (5):573–577.

المخلص العربي

التأثير العلاجي المحتمل للخلايا الجذعية الوسيطة وحوصلاتها الدقيقة على اعتلال الشبكية السكري المستحث تجريبياً في الجرذان دراسة هستولوجية وهستوكيميائية مناعية

هبة السيد عبد الحليم، أميمة كامل هلال، نسرین ابراهيم سالم ونهله العراقي العزب

قسم الأنسجة وبيولوجيا الخلية - كلية الطب - جامعة بنها

المقدمة: يعتبر اعتلال الشبكية السكري هو أحد مضاعفات الأوعية الدموية الدقيقة لمرض السكري التي تهدد البصر وتصيب شبكية العين. ومع تطور التكنولوجيا الطبية الحديثة في مجال العلاج الخلوي، أصبح العلاج بالخلايا الجذعية والحوصلات الدقيقة يمثل استراتيجيات علاجية واعدة لمرض اعتلال الشبكية السكري.

الهدف من البحث: تقييم التأثير العلاجي المحتمل للخلايا الجذعية الوسيطة وحوصلاتها الدقيقة على اعتلال الشبكية السكري الناتج في الجرذان.

الطريقة وخطة العمل: تضمنت هذه الدراسة عشرة جرذان صغيرة لتحضير الخلايا الجذعية الوسيطة، و عدد أربعة وستون من ذكور الجرذان البالغة. تم تقسيم الجرذان البالغة إلى ستة مجموعات. المجموعة الأولى (الضابطة). المجموعة الثانية (المجموعة المتأثرة): تلقت الجرذان حقنة واحدة داخل التجويف البريتوني (٦٠ مغ / كغ من وزن الجسم) من عقار ستريبتوزوتوسين المذاب حديثاً في محلول سترات. المجموعة الثالثة: مجموعة اعتلال الشبكية السكري المعالج بالخلايا الجذعية الوسيطة. المجموعة الرابعة: مجموعة اعتلال الشبكية السكري المعالج بالحوصلات الدقيقة المستمدة من الخلايا الجذعية الوسيطة للنخاع العظمي. المجموعة الخامسة: مجموعة اعتلال الشبكية السكري المعالج بالخلايا الجذعية الوسيطة مع حوصلاتها الدقيقة. المجموعة السادسة: المجموعة المتعافية. أخذت عينات شبكية العين وتمت معالجتها و تحضيرها للدراسة الهستولوجية والهستوكيميائية المناعية.

النتائج: أظهرت المجموعة الثانية والسادسة انخفاض ملحوظ في سماكة الشبكية، واضطراب واضح للجزء الخارجي من مستقبلات الضوء، مع تجويفات سيتوبلازمية في خلايا الطبقات النووية الداخلية و الطبقة العقدية. علاوة على ذلك، كان هناك زيادة ذو دلالة احصائية في تفاعل بروتين عامل نمو بطانة الأوعية الدموية وبروتين الفيمنتين ($P > 0,05$). أظهرت المجموعتان الثالثة والرابعة تحسناً لبعض التغييرات الهستولوجية التي وصفت في المجموعة الثانية. في حين، أظهرت المجموعة الخامسة البنية الهستولوجية والتركيب الدقيق قريبين من المجموعة الضابطة.

الاستنتاج: يمكن للخلايا الجذعية الوسيطة وحوصلاتها الدقيقة علاج اعتلال الشبكية السكري. ومع ذلك، يمكن الحصول على نتائج أفضل عندما يتم إعطاء الخلايا الجذعية الوسيطة مع حوصلاتها الدقيقة.